Martin Marietta Laboratories

MARTIN MARIETTA

MOLECULAR INTERACTIONS AT METAL/POLYIMIDE INTERFACES: A CORRELATION WITH ADHESION AND BOND DURABILITY

G.D. DAVIS, B.J. REES AND P.L. WHISNANT
MARTIN MARIETTA LABORATORIES • BALTIMORE
BALTIMORE, MD 21227-3898

K.M. LIECHTI AND A. SHIRANI
DEPARTMENT OF AEROSPACE ENGINEERING AND ENGINEERING MECHANICS
UNIVERSITY OF TEXAS
AUSTIN, TX 78712

ANNUAL REPORT
FOR ONR CONTRACT N00014-C-92-0004

FEBRUARY 1994

Unclassified
SECURITY CLASSIFICATION OF THIS PAGE

REPORT DOCUMENTATION PAGE

1a REPORT SECURITY CLASSIFICATION: Unclassified

1b RESTRICTIVE MARKINGS: None

2a SECURITY CLASSIFICATION AUTHORITY

2b DECLASSIFICATION / DOWNGRADING SCHEDULE: None

3 DISTRIBUTION / AVAILABILITY OF REPORT: Unlimited

4 PERFORMING ORGANIZATION REPORT NUMBER(S): MML TR 94-08

5 MONITORING ORGANIZATION REPORT NUMBER(S)

6a NAME OF PERFORMING ORGANIZATION:
Martin Marietta Corporation
Martin Marietta Laboratories

6b OFFICE SYMBOL *(If applicable)*: MML

7a NAME OF MONITORING ORGANIZATION:
Defense Contract Administration Services
Management Area - Baltimore

6c ADDRESS *(City, State, and ZIP Code)*:
1450 S. Rolling Road
Baltimore, MD 21227-3898

7b ADDRESS *(City, State, and ZIP Code)*:
300 East Joppa Road
Baltimore, MD 21204-3099

8a NAME OF FUNDING / SPONSORING ORGANIZATION: Office of Naval Research

8b OFFICE SYMBOL *(If applicable)*: ONR

9 PROCUREMENT INSTRUMENT IDENTIFICATION NUMBER: N00014-93-C-004

8c ADDRESS *(City, State, and ZIP Code)*:
800 North Quincy Street
Arlington, VA 22217-5000

10 SOURCE OF FUNDING NUMBERS

PROGRAM ELEMENT NO.	PROJECT NO.	TASK NO	WORK UNIT ACCESSION NO

11 TITLE *(Include Security Classification)*: Molecular Interactions at Metal/Polyimide Interfaces: A Correlation with Adhesion and Bond Durability

12 PERSONAL AUTHOR(S): G.D. Davis, B.J. Rees, P.L. Whisnant, K.M. Liechti, and A. Shirani

13a TYPE OF REPORT: Annual

13b TIME COVERED: FROM 11/1/92 TO 10/31/9

14 DATE OF REPORT *(Year, Month, Day)*: 1994 February 18

15 PAGE COUNT: 37

16 SUPPLEMENTARY NOTATION

17 COSATI CODES

FIELD	GROUP	SUB-GROUP

18 SUBJECT TERMS *(Continue on reverse if necessary and identify by block number)*: Approved for public release; distribution unlimited. Reproduction in whole or in part is permitted for any purpose of the United States Government.

19 ABSTRACT *(Continue on reverse if necessary and identify by block number)*

Molecular interactions between a substrate and an overlayer control the intrinsic adhesion between the two materials and this intrinsic adhesion, in turn, is a critical component of the measured adhesion which also includes factors related to plastic deformation of the materials. Because virtually all measurements of adhesion include these other factors, accurate values for the intrinsic adhesion have not been available in the past. To develop a means to measure this parameter, nonlinear von Karman plate theory has been used for a consistent analysis of pressurized circular, island and peninsula blister specimens. The configurations considered ranged from linear plates to membranes. Interfacial energy release rates and fracture mode-mixes were extracted. For a given pressure and all possible materials and delamination length to thickness (aspect, a/h) ratios, the peninsula blister provided the highest energy release rate, followed by the island and circular blisters. The extent of yielding in delaminating copper films was greatest with the circular blister. The stress levels in the island blister were notably lower. While extensive yielding was still present in peninsula blister configurations with a/h = 100 and 500, there was none for a/h = 10. A scheme for extending the utility of blister specimens to higher aspect ratios was developed and analyzed.

In preparation for correlating intrinsic adhesion with chemical interfacial bonding, the interactions of copper overlayers with four different polyimides [pyromellitic dianhydride - oxydianiline (PMDA-ODA), benzophenonetetra-carboxylic dianhydride - diaminobenzophenone (BTDA-DABP); oxydiphthalic anhydride - oxydianiline (ODPA-ODA); and pyromellitic dianhydride - phenylene diamine (PMDA-PDA)] were studied by XPS. Emergent ether-like functionalities on polyimides without innate ether groups suggested a copper-induced partial reduction of carbonyl groups. A surface behavior diagram of the carbon chemistry confirmed this reaction by indicating a partial replacement of carbonyl moieties with ether-like moieties.

20 DISTRIBUTION / AVAILABILITY OF ABSTRACT: ☐ UNCLASSIFIED/UNLIMITED ☐ SAME AS RPT ☐ DTIC USERS

21 ABSTRACT SECURITY CLASSIFICATION: Unclassified

22a NAME OF RESPONSIBLE INDIVIDUAL: Dr. Guy D. Davis

22b TELEPHONE *(Include Area Code)*: (410) 204-2376

22c OFFICE SYMBOL

DD FORM 1473, 84 MAR
83 APR edition may be used until exhausted
All other editions are obsolete

SECURITY CLASSIFICATION OF THIS PAGE

U.S. Government Printing Office 1986—607-044

MOLECULAR INTERACTIONS AT METAL/POLYIMIDE INTERFACES: A CORRELATION WITH ADHESION AND BOND DURABILITY

G.D. Davis, B.J. Rees, and P.L. Whisnant
Martin Marietta Laboratories
Baltimore, MD 21227

K.M. Liechti and A. Shirani
Department of Aerospace Engineering and Engineering Mechanics
University of Texas
Austin, TX 78712

Annual Report
for ONR Contract N00014-C-92-0004

February 1994

LIST OF FIGURES ii

ABSTRACT 1

INTRODUCTION 2

EXPERIMENTAL 4

STRESS ANALYSIS 9
INTERFACE ANALYSIS 8

RESULTS AND DISCUSSION 9

STRESS ANALYSIS 9
FABRICATION PROCEDURE 22
INTERPHASAL CHEMISTRY 23

SUMMARY AND CONCLUSIONS 32

ACKNOWLEDGMENTS 32

REFERENCES 33

LIST OF FIGURES

FIGURE		PAGE
1.	Repeat unit of the polyimides investigated.	3
2.	Blister Specimen Geometries.	5
3.	Central Deflections of the Circular, Island and Peninsula Blister Specimens.	10
4.	Energy Release Rates Available from Circular, Island and Peninsula Blister Specimens.	10
5.	Fracture Mode-Mixes Associates with Circular, Island and Peninsula Blister Specimens.	11
6.	Critical Pressures in Circular, Island and Peninsula Blister Specimens for an Interfacial Toughness of 100 J/m^2.	12
7.	Maximum von Mises Effective Stresses in Circular, Island and Peninsula Blister Specimens.	13
8.	Von Mises Effective Stress Distribution in (a) Plate, (b) Transition and (c) Membrane Configurations of the Circular Blister.	14
9.	Von Mises Effective Stress Distribution in (a) Plate, (b) Transition and (c) Membrane Configurations of the Island Blister.	15
10.	Longitudinal Von Mises Effective Stress Distribution in (a) Plate, (b) Transition and (c) Membrane Configurations of the Peninsula Blister.	16
11.	Spanwise Von Mises Effective Stress Distribution in (a) Plate, (b) Transition and (c) Membrane Configurations of the Peninsula Blister.	17
12.	Von Mises Effective Stress Contours in Peninsula Blisters with Aspect Ratios (a) $a/h = 10$, and (b) $a/h = 100$.	19
13.	Longitudinal and Spanwise Distributions of von Mises Effective Stresses in a Composite Peninsula Blister.	21
14.	Carbon and oxygen 1s spectra for clean polyimides.	24
15.	Carbon and oxygen 1s spectra of PMDA-PDA for a clean substrate and after deposition of approximately 0.3 and 3 nm of copper.	25
16.	Normalized concentrations of carbonyl and ether oxygen as a function of copper concentration.	26
17.	Normalized concentrations of carbonyl and ether carbon as a function of copper concentration.	27
18.	FWHM of Cu $2p_{3/2}$ peak as a function of copper concentration.	29
19.	FWHM of O 1s carbonyl and ether peaks as a function of copper concentration.	29
20.	FWHM of C 1s carbonyl and ether peaks as a function of copper concentration.	30
21.	Surface behavior diagram tracing the evolution of the carbon chemistry as a function of copper concentration for PMDA-PDA and PMDA-ODA. The numbers beside each peak represent the atomic concentration of copper.	31

ABSTRACT

Molecular interactions between a substrate and an overlayer control the intrinsic adhesion between the two materials and this intrinsic adhesion, in turn, is a critical component of the measured adhesion which also includes factors related to plastic deformation of the materials. Because virtually all measurements of adhesion include these other factors, accurate values for the intrinsic adhesion have not been available in the past. To develop a means to measure this parameter, nonlinear von Karman plate theory has been used for a consistent analysis of pressurized circular, island and peninsula blister specimens. The configurations considered ranged from linear plates to membranes. Interfacial energy release rates and fracture mode-mixes were extracted. For a given pressure and all possible materials and delamination length to thickness (aspect, *a/h*) ratios, the peninsula blister provided the highest energy release rate, followed by the island and circular blisters. The extent of yielding in delaminating copper films was greatest with the circular blister. The stress levels in the island blister were notably lower. While extensive yielding was still present in peninsula blister configurations with *a/h = 100* and *500*, there was none for *a/h = 10*. A scheme for extending the utility of blister specimens to higher aspect ratios was developed and analyzed.

In preparation for correlating intrinsic adhesion with chemical interfacial bonding, the interactions of copper overlayers with four different polyimides [pyromellitic dianhydride - oxydianiline (PMDA-ODA), benzophenonetetracarboxylic dianhydride - diaminobenzophenone (BTDA-DABP); oxydiphthalic anhydride - oxydianiline (ODPA-ODA); and pyromellitic dianhydride - phenylene diamine (PMDA-PDA)] were studied by XPS. Emergent ether-like functionalities on polyimides without innate ether groups suggested a copper-induced partial reduction of carbonyl groups. A surface behavior diagram of the carbon chemistry confirmed this reaction by indicating a partial replacement of carbonyl moieties with ether-like moieties.

INTRODUCTION

The measured adhesion of an overlayer/substrate system can be considered to have two components, an intrinsic adhesion controlled by chemical and physical interactions between a substrate and an overlayer and a multiplicative factor that includes the plastic deformation or yielding of the overlayer during the delamination. This multiplicative factor is commonly much larger than unity but is dependent on the materials of the system, the type of stresses applied, the rate at which they are applied, and the environment to which the system has been exposed. Hence, any measurement of adhesion depends on the process by which the value has been obtained.

The increase in measured adhesion strength over the intrinsic interfacial adhesion has great practical advantages when one is attempting to maximize adhesion. Nonetheless, the intrinsic adhesion or fracture toughness is critical because without a strong interface/interphase, no deformation of materials will occur and the bonded system will fail readily. Despite the importance of this parameter and the need to correlate it with chemical and physical bonds across the interface, its measurement has been elusive because of the nearly universal yielding of materials during testing. In this program, we are attempting to determine the intrinsic fracture toughness of an interface and compare it with interfacial chemical bonding.

Our correlation of chemical interphasal bonding with interphasal fracture toughness entails four tasks: stress analysis of different test configurations to design a specimen exhibiting no inelastic deformation during testing; development of a procedure to fabricate these specimens; determination of the interphasal chemical interactions; and measurement of the interphasal fracture toughness. The first two of these tasks are highly interactive as the final test specimen needs to be both analyzable and producible. Considerable progress has been made on the first three tasks and are reported here.

We have chosen the copper/polyimide system for this study. It has significant technological applications in the microelectronics industry and the interactions of various metals with pyromellitic dianhydride - oxydianiline (PMDA-ODA) have been widely studied.[1-16] For our purposes, the copper/polyimide system is ideal in that the chemical bonds formed are relatively weak so that failure can be forced interfacially with little probability of crack propagation within the polymer or metal; smooth interfaces can be formed that will contribute no physical (mechanical) bonding; and test specimens can be fabricated using standard electronic device processing techniques.

Most investigators have concluded that reactive metals initially interact with the carbonyl groups of the polyimide.[1-11] However, interactions with the aromatic rings have also been proposed[12-14] as has the possibility that reactive, e.g., Cr, Ti, Co, and Al, and unreactive, e.g., Cu, Ag, and Au, metals will interact with different sites.[3,12,14] It is expected that a concomitant result of this work will be an improved understanding of the interactions of copper deposited onto polyimide substrates.

The polyimides that have been investigated were chosen to provide differing concentrations of carbonyl and ether moieties on both the dianhydride and diamine components of the polyimide: PMDA-ODA, the microelectronics standard; benzophenonetetracarboxylic dianhydride - diaminobenzophenone (BTDA-DABP) with two phenyl rings joined by carbonyl groups on each component; oxydiphthalic anhydride - oxydianiline (ODPA-ODA) with two phenyl rings joined by ether groups on each component; and pyromellitic dianhydride - phenylene diamine (PMDA-PDA) with only one phenyl ring in each component. They are shown in Figure 1 and the concentrations of the various groups are given in Table 1.

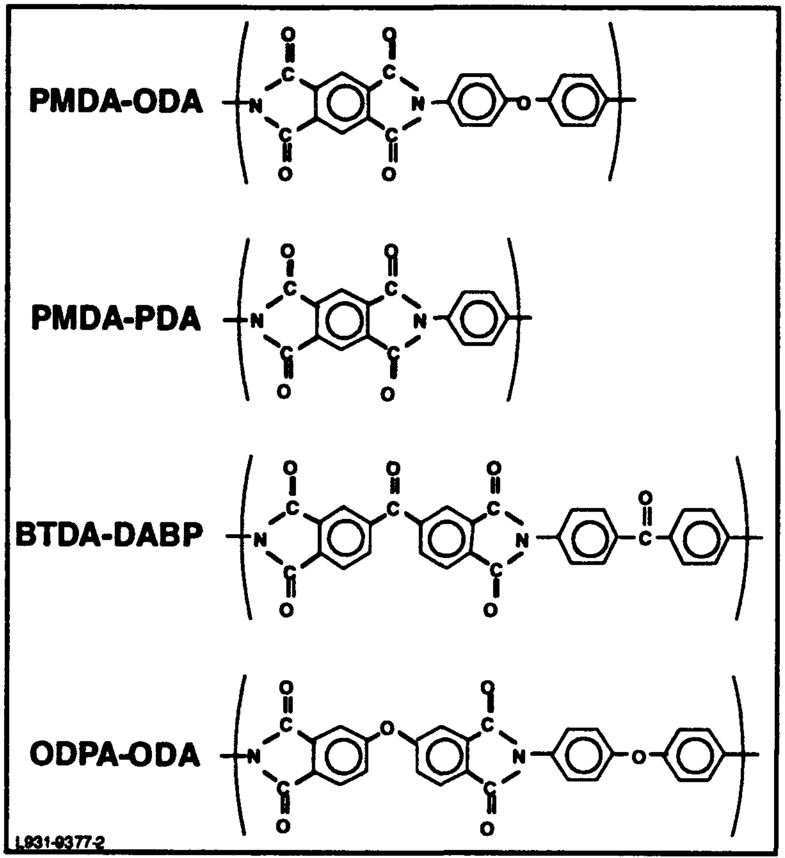

Figure 1. Repeat unit of the polyimides investigated.

Table 1. Calculated Atomic Concentrations of Various Chemical States in Polyimides

polyimide	C-O-C	C=O	N	C=O	C-O	C-N	C-C dianhydride	C-C diamine
PMDA-PDA	0	18.2	9.1	18.2	0	9.1	27.3	18.2
BTDA-DABP	0	15.8	5.3	15.8	0	5.3	31.6	26.3
ODPA-ODA	5.6	11.1	5.6	11.1	11.1	5.6	27.8	22.2
PMDA-ODA	3.4	13.8	6.9	13.8	6.9	6.9	19.7	27.6

One method of quantifying the resistance to delamination is to use a fracture mechanics approach with blister specimens. Blister specimens have been used for examining delamination mechanisms in relatively thick layers since the early works of Dannenberg,[17] Willliams and co-workers,[18-23] Takashi et al.,[24,25] and Erdogan and Arin.[26] Reference 27 contains a review of the material combinations and specimen configurations that had been examined and analyzed up to the mid 1980's. It was about that time that interest in using the pressurized circular blister test for microelectronic applications arose[28] and a membrane analysis[29] was proposed. As tougher interfaces were examined, problems were encountered with tensile failure in the blistering film prior to delamination.[30] This motivated the development of several alternative configurations such as the island blister,[31] the constrained blister,[32,33] and the peninsula blister.[34] Linear plate and approximate membrane analyses that sometimes account for residual stresses have been used to delineate the advantageous regimes of operation of each configuration. The most recent arrival, the peninsula blister,[34] shows most promise due to the relatively low pressure levels required to produce delamination and the fact that it is a constant energy release rate configuration. However, based on recent experiments with blister specimens,[35] it is not enough to have the delaminating film survive the test; the amount of yielding in the delaminating layer should be limited so that linear elastic analyses can be properly conducted. Otherwise, elastoplastic analyses, such as the one by Kim and Aravas[36] for thin film peeling, will have to be conducted in order to account for dissipative effects due to large scale yielding.

To determine the feasibility of using these specimens to measure interfacial fracture toughness, we have analyzed the behavior of pressurized circular, island and peninsula blister specimens in a consistent manner over a wide range of delamination length to thickness ratios and provide a measure of the extent of yielding that can be expected to occur in each specimen for a given interfacial toughness. The specimens were analyzed and their responses were compared on the consistent basis of nonlinear von Karman plate theory[37] which has as special cases the limiting behavior of membranes and linear plates. Such an analysis of the circular blister has recently been conducted[38] with a sequel that has included residual stress effects.[39]

EXPERIMENTAL

STRESS ANALYSIS

The geometries of the specimens that are being compared in this study are shown in Figure 2. In all cases, we considered that a copper layer had been deposited on polyimide which, in turn, had already been deposited on a convenient substrate. A delamination was placed between the copper and polyimide layers, leaving a blister of thickness, *h*, and a planform geometry that reflected the type of specimen. The simplest is the circular blister with a debond diameter of *2a*. The debond in the island blister is annular with an inside diameter of *2b* and outside diameter of *2a*. Delamination proceeds by decreasing the inside diameter or the size of the island.[31] The delaminating layer in the peninsula blister specimen has a rectangular planform of length, *a*, and span, *2c*. It is essentially attached to the polyimide layer along $y = \pm c$, along $x = 0$ for $|y| \le c$ and along $x = a$ for $|y| < b$. Under certain conditions,[34] delamination will only progress along the length of the peninsula, increasing the length, *a*. In the results presented later, the delaminations were fixed at $a = 5mm$ while the thickness of the delaminating layer had the range $0.005 \le h \le 0.5mm$. The island and peninsula blisters had the same ratio of propagating to stationary delamination front length ($b/a = c/b = 0.1$) and the delamination span to length ratio for the peninsula blister was $c/a = 0.5$. In all cases, a pressure, *p*, is applied to the faces of the delamination through a port in the substrate, S. As a first step and also because most of the strain energy available to produce fracture is stored in the copper layer, it was considered to be rigidly clamped along the boundaries of the delamination, essentially ignoring any deformation in the polyimide layer.

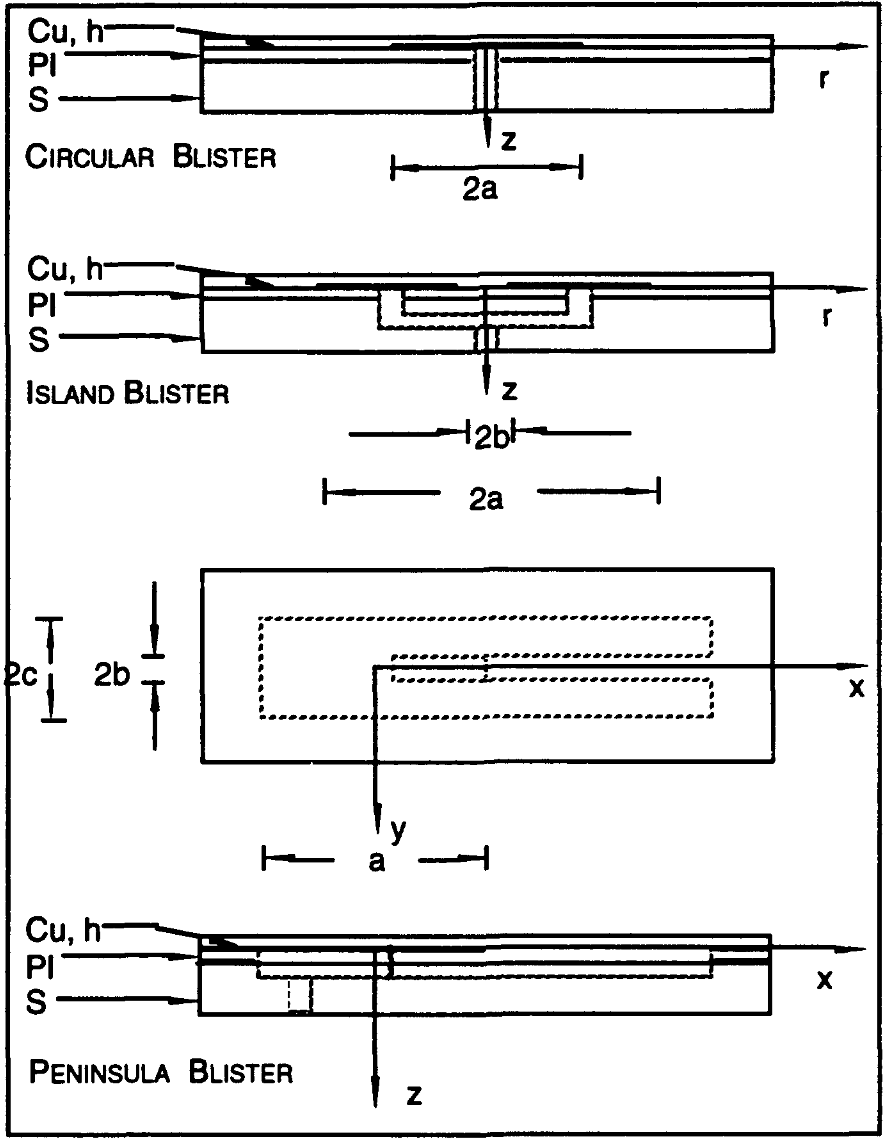

Figure 2. Blister Specimen Geometries.

In the past, various stress analyses have been conducted of the geometries shown in Figure 2. These have focused on the two extremes of linear plate and membrane behavior. However, some of the delamination sizes and copper layer thicknesses being considered here put the response in the transition between linear plate and membrane behavior. It was therefore necessary to conduct the stress analyses on the basis of von Karman plate theory[37] that accounts for bending and stretching of the delaminating film under large deflections. Although the latter give rise to nonlinear effects, the strains are small and the material response was therefore taken to be linearly elastic, with Young's modulus, *E*, and Poisson's ratio, ν. Subsequent analyses may have to account for nonlinear material behavior.

Because of their circular nature, the field equations for the circular and island blisters were expressed in cylindrical coordinates, *r*, θ, and *z*, with corresponding displacements *u*, *v*, and *w*. However, because of the axisymmetric nature of the geometries and loadings, displacements (and hence strains and stresses) are independent of θ and $v = 0$. We introduced the nondimensional quantities:

$$\rho = r/a \text{ and } \overline{w} = w/h \tag{1}$$

and used

$$p_o = \frac{16}{3} \cdot \frac{E}{1-\nu^2}\left(\frac{h}{a}\right)^4 \tag{2}$$

for nondimensionalizing pressures.

The stresses in the layer were expressed in terms of the stress resultants N_r and N_θ where

$$N_r = \int_{-h/2}^{h/2} \sigma_r \, dz \text{ and } N_\theta = \int_{-h/2}^{h/2} \sigma_\theta \, dz. \tag{3}$$

and the bending moments

$$M_r = \int_{-h/2}^{h/2} \sigma_r \, z \, dz \text{ and } M_\theta = \int_{-h/2}^{h/2} \sigma_\theta \, z \, dz. \tag{4}$$

The stress resultants can be derived from a stress function, ϕ, through

$$N_r = \frac{\phi}{r} \text{ and } N_\theta = \frac{d\phi}{dr}. \tag{5}$$

Consideration of equilibrium and compatibility leads to two simultaneous, differential equations in $\overline{w}$ and $\overline{\phi} = a\,\phi / Eh^3$, the nondimensionalized ϕ,

$$\rho\,\overline{\phi}'' + \overline{\phi}' - \overline{\phi}/\rho = -\frac{1}{2}\,\overline{w}'^2 \tag{6}$$

$$\rho^2\,\overline{w}''' + \rho\,\overline{w}'' - \overline{w}' = -32\left(p/p_o\right)\rho^3 + 12\left(1-\nu^2\right)\rho\,\overline{\phi}\,\overline{w}' \tag{7}$$

where $(\;)' \equiv \frac{d(\;)}{d\rho}$, $(\;)'' = \frac{d^2(\;)}{d\rho}$, etc.

The boundary conditions for the circular blister were taken to be

$$\bar{w}'(0) = \bar{\phi}(0) = 0 \tag{8}$$

and

$$\bar{w}(1) = \bar{w}'(1) = \bar{\phi}'(1) - \nu\bar{\phi}(1) = 0. \tag{9}$$

The conditions on $\bar{\phi}$ at r = 0 and 1 reflect the requirements of finite stresses and zero radial displacement, respectively.

Although the governing equations for the island blister are the same as those of the circular blister, convergent solutions were more easily obtained when the origin of the coordinate system was moved to the center of the annular region. The nondimensional quantities were also changed to reflect the island blister geometry so that

$$\rho = 2r/(a-b), \quad \bar{w} = w/h \quad \text{and} \quad \bar{\Phi} = \phi(a-b)/Eh^3$$

The quantity $\xi = 1 - \rho$ was used to represent the translation of the coordinate system, in which case the governing equations became

$$(1-\xi)\bar{\Phi}'' - \bar{\Phi}' - \phi/(1-\xi) = -\tfrac{1}{2}\bar{w}'' \tag{10}$$

$$(1-\xi)\bar{w}''' - \bar{w}'' - \bar{w}'/(1-\xi) = 6(1-\nu^2)\bar{\Phi}\bar{w}' - \frac{2p}{p_o}\left[(1-\xi)^2 - 1\right](1-b/a)^4. \tag{11}$$

The boundary conditions at $\xi = 0$ were

$$\bar{w}'(0) = \bar{\phi}'(0) + \nu\bar{\phi}(0) = 0 \tag{12}$$

reflecting zero slope and radial displacement at the center of the deflected region. Along the debond front

$$\bar{w}(1) = \bar{w}'(1) = \bar{\phi}'(1) + \nu\bar{\phi}(1) = 0. \tag{13}$$

Once the displacement was determined, the bending moment was obtained through the stress strain behavior from

$$M = \frac{Eh^3}{12(1-\nu^2)}\left(w'' + \nu w'/r\right). \tag{14}$$

The rectangular planform of the blistered areas in the peninsula specimen suggests the x, y, z Cartesian coordinate system shown in Figure 2, with corresponding displacements u, v, w. The governing equations were

$$D\nabla^4 w - q - h\left(w_{,xx}F_{,yy} + w_{,yy}F_{,xx} - 2w_{,xy}F_{,xy}\right) = 0 \tag{15}$$

$$\nabla^4 F = E\left(w_{,xy}^2 - w_{,xx}w_{,yy}\right) \tag{16}$$

The fully clamped boundaries led to the conditions

$$u = w = w_{,x} = F_{,xy} = 0 \qquad x = \pm a/2 \tag{17}$$

$$v = w = w_{,y} = F_{,xy} = 0 \qquad y = \pm c/2. \tag{18}$$

The equations for the circular and island blister were converted to a series of simultaneous first order ordinary differential equations and solved numerically. A Raleigh Ritz procedure was used to obtain the solution for the peninsula blister deflection, *w*. The procedure was checked against the solution for the one dimensional case, which was obtained analytically. Once *w* was determined, the bending moment, *M*, the membrane force resultant, *N*, and the stress, σ, could be found at any location along and through the thickness of the copper. For the circular and island blisters, the energy release rate, *G*, was extracted from the values of *M* and *N* at the crack front.[40]

$$G = \frac{6\,(1-\nu^2)}{Eh^3}\left[M^2 + \frac{h^2N^2}{12}\right]. \tag{19}$$

The normalizing energy release that was used later in Figure 3 was taken to be

$$G_0 = \frac{Eh^5}{(1-\mathrm{v}^2)a^4} \tag{20}$$

The fracture mode-mix is expressed as the angle

$$\begin{aligned} \psi &= \tan^{-1}\left\{\frac{\mathrm{Im}(Kh^{i\varepsilon})}{\mathrm{Re}(Kh^{i\varepsilon})}\right\} \\ \psi &= \frac{\sqrt{12}M\cos\omega + hN\sin\omega}{-\sqrt{12}M\sin\omega + hN\cos\omega} \end{aligned} \tag{21}$$

where $K = K_1 + i\,K_2$ is the complex interfacial stress intensity factor which gives the stresses ahead of the crack through

$$\sigma_r + i\sigma_{rz} = \frac{K}{\sqrt{2\pi r}}\,r^{i\varepsilon}\ . \tag{22}$$

The angle ω depends on the Dundurs' parameters *a* and *b* and ε is the bimaterial constant

$$\varepsilon = \frac{1}{2\pi}\ln\frac{1-\beta}{1+\beta}\,. \tag{23}$$

A universal plot of ω vs. α for $\beta = 0$, $\alpha/4$, and $\alpha/2$ is given by Hutchinson and Suo.[40]

An alternative scheme for determining the energy release rate provided by the peninsula blister had to be used because there are three regions that are pressurized. The energy released comes from the two regions ahead of the crack front on either side of the peninsula ($a \le x \le \ell$; $b \le |y| \le c$), while some is still stored in the one region behind the crack front ($x \le a$; $|y| \le c$). The potential energy of the three blistering regions is

$$\Pi = \Pi_1 a + \Pi_2(\ell - a)\,. \tag{24}$$

The energy release rate, *G*, is given by the rate of change of potential energy with increasing crack area, so that

$$G = -\frac{1}{2b}\,\frac{\partial\Pi}{\partial a} = \frac{(\Pi_2 - \Pi_1)}{2b}\,. \tag{25}$$

INTERFACE ANALYSIS

The poly(amide acid) precursors were synthesized from pure monomers in a closed vessel at room temperature under nitrogen using N,N-dimethylacetamide.[41] The poly(amide acids) were spun coat onto a silicon wafer and cured at 140°C for 0.5 hours, cooled to room temperature, and cured at 300°C for 1 hour. Wafers were cleaved into four pieces and stored in a dessicator until use. Each specimen was inserted into the vacuum chamber via a load lock one to three days prior to deposition experiments. The base pressure of the chamber was in the low 10^{-7} Pa range.

X-ray photoelectron spectroscopy (XPS) measurements were made on the clean polyimides and after deposition of copper to various levels using a Surface Science Laboratories SSX100 spectrometer with a hemispherical electron analyzer with multichannel detection and a monochromatized Al x-ray source focused to 600µm. To minimize or eliminate differential charging yet allow unimpeded deposition, a retractable screen was designed to allow placement directly over the surface during XPS analysis when needed and removal during transfer to the evaporation station.[42] Survey spectra and high-resolution spectra of the Cu 2p, O 1s, N 1s, and C 1s peaks were acquired on the clean specimen and after deposition of 0.1, 0.3, 1, 3, and 10 nm Cu. A Shirley background subtraction was used for quantification and curve fitting unless a small peak on top of a sloping background required a linear background. Curve fitting was achieved using the manufacturer's software. Although peak width and energy were not fixed, they were examined to assure consistency within a run and from sample to sample. The greatest uncertainty in the curve fitting involved the two aromatic carbon peaks from the dianhydride and diamine components and the ether peak because of their overlap. Quantification was obtained from the curve fitted peaks using sensitivity factors derived from standards. Intensity of the carbon and oxygen shake-up satellites were proportioned between the aromatic carbon peaks and the two oxygen peaks, respectively prior to quantification. Binding energies were normalized to the carbonyl O 1s at 532.3 eV for clean substrates and to Cu $2p_{3/2}$ at 932.7 eV for surfaces after depositions.

Depositions were made in an attached preparation chamber using an electron-beam evaporator. Thicknesses were monitored using a quartz crystal oscillator. Deposition rates were usually 0.02-0.1 nm/s, depending on the desired incremental deposition.

RESULTS AND DISCUSSION

STRESS ANALYSIS

Dimensionless values of central deflection, energy release rate and fracture mode-mix will first be compared as a function of a dimensionless pressure. These results can then be used to examine the response of any combination of specimen geometry and material selection. The comparison will then be made more specific in order to compare stress levels and distributions in a layer of copper delaminating from an interface with a toughness of $100\ J/m^2$.

The central deflections of the three specimens are shown in Figure 3, under the designations CB, IB and PB, for circular, island and peninsula blisters, respectively. It can be seen that the response was quite nonlinear with values up to 25 layer thicknesses being achieved for the pressure range considered. The most compliant response was that of the circular blister, followed by those of the island and peninsula blisters. Smaller values of *b/a* for the island blister or *b/c* for the peninsula blister produced even lower deflections.

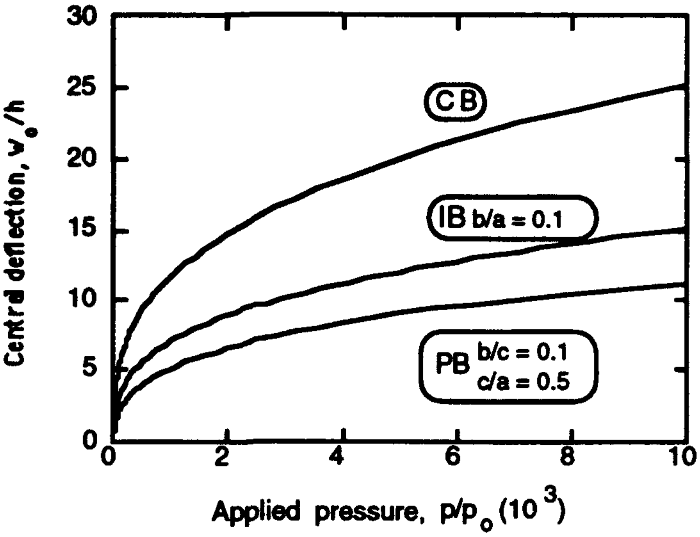

Figure 3. Central deflections of the circular, island and peninsula blister specimens.

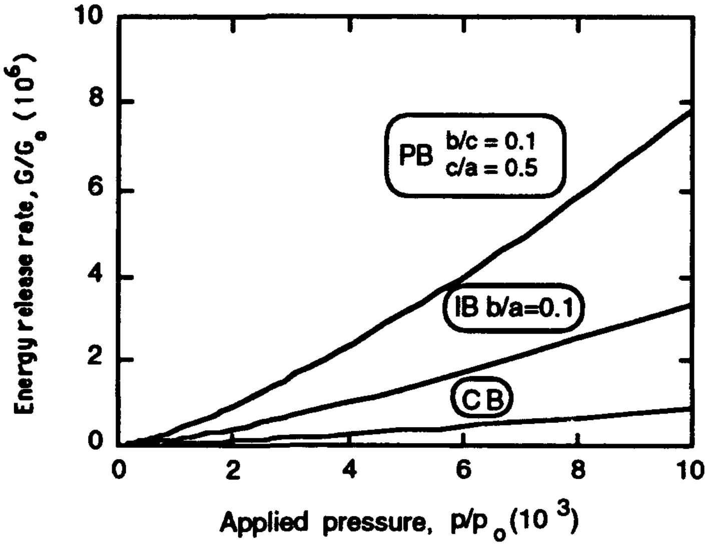

Figure 4. Energy release rates available from circular, island and peninsula blister specimens.

The next step was to compare the energy release rates that each specimen could provide for a given pressure (Figure 4). The principal advantage of the peninsula blister, namely that it provides relatively high energy release rates, is clearly demonstrated over the full range of pressures. As pointed out in

Reference 34, this is due to the relatively small debonding area compared to that of the circular blister. Again, decreases in *b/a* or *b/c* would lead to even higher energy release rate values for the island and peninsula blisters.

In view of the variation of interfacial toughness with fracture mode-mix that has now been noted for a wide range of materials,[43-47] an important step in characterizing the response of any fracture property specimen is the range of mode-mixes that it provides. The values that can be obtained from the three specimens being considered here are shown in Figure 5. In all cases, especially at lower pressures, the mode-mix varied quite strongly with pressure level. The values were all negative, which seems to be a general characteristic of blister specimens. For each specimen, the mode-mix values ranged over about 10 to 15 degrees for the pressure levels that were considered. In addition, there was a notable difference in mode-mix values from specimen to specimen.

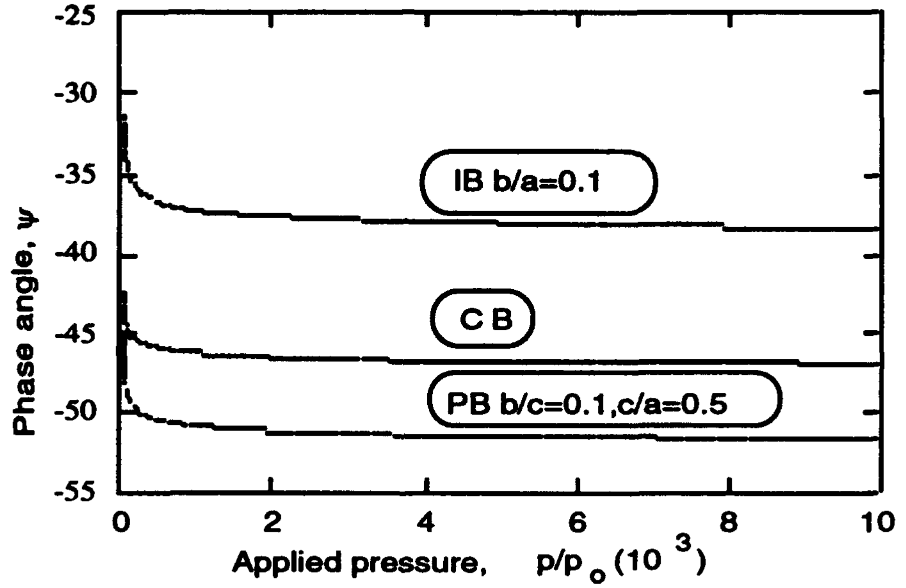

Figure 5. Fracture mode-mixes associates with circular, island and peninsula blister specimens.

A key task of the program is to design fracture property specimens that would allow the fracture properties to be extracted in a relatively straightforward manner, using linear elastic fracture mechanics concepts. This means that the amount of plastic deformation in the delaminating layer should be limited to region near the crack front that is smaller than the delaminating layer thickness. A second factor of interest was the range of pressures that should be applied to cause delamination so that pressurization equipment and transducers could be chosen appropriately. An interfacial fracture toughness of *100* J/m^2 was chosen as the main design parameter.

The critical pressures predicted by the nonlinear von Karman plate theory for the three blister specimens are shown in Figure 6. All the responses shown exhibited the power law extremes of linear plate and membrane behavior with a transition region between them, as the crack length to delaminating layer thickness increased. As expected from the results shown in Figure 4, the circular blister would require the highest pressures, followed by the island and peninsula blister specimens. For *10 < a/h < 1000*, it can be seen that critical pressure levels in the circular blister ranged from about 900 to 60 psi and linear plate and membrane theories can be used for *a/h < 20* and *a/h > 100*, respectively. The transition regions for the other two specimens shifted to higher *a/h* values, mainly due to differences in membrane response. The pressure range for the peninsula blister was from 500 to 20 psi for *10 < a/h < 1000.*

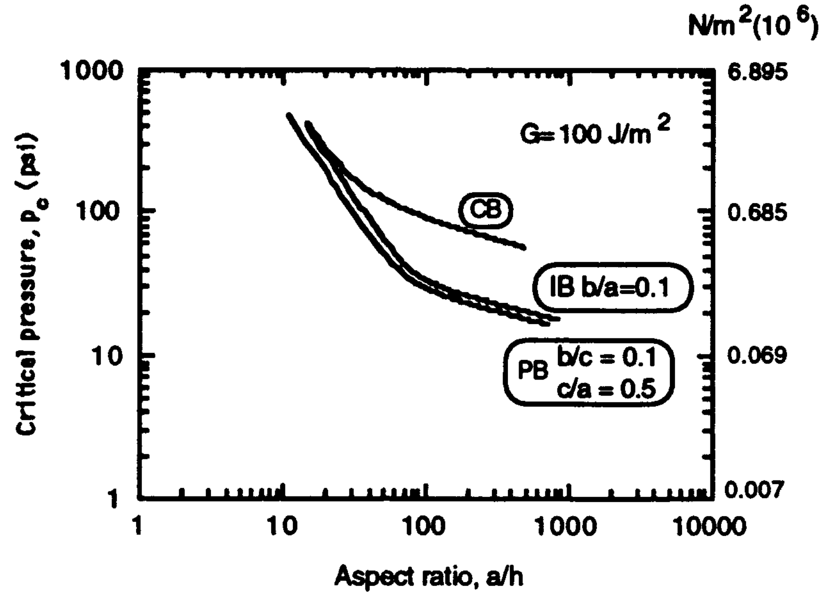

Figure 6. Critical pressures in circular, island and peninsula blister specimens for an interfacial toughness of 100 J/m^2.

The issue of yielding in the delaminating layer was examined in two ways. The first was to compare the maximum levels of the von Mises effective stress, e, at the critical pressure over the full range of *a/h* values that have been considered in previous figures. There was the expected result that the thinner the delaminating layer thickness is, the higher the maximum stresses become (Figure 7). For the circular and island blisters, the maximum stresses ranged from 7 to 80 times the yield strength of copper. The effective stress levels in the peninsula blister were considerably lower than those in the other two configurations and their distribution was more sensitive to the aspect ratio in that there was a more obvious transition from plate to membrane behavior. The stress levels in Figure 7 are conservative in the sense that the analysis that yielded them would not account for singular stresses that occur along the delamination front. However, even without the singular behavior, it is clear that relatively large stresses can develop near the delamination front.

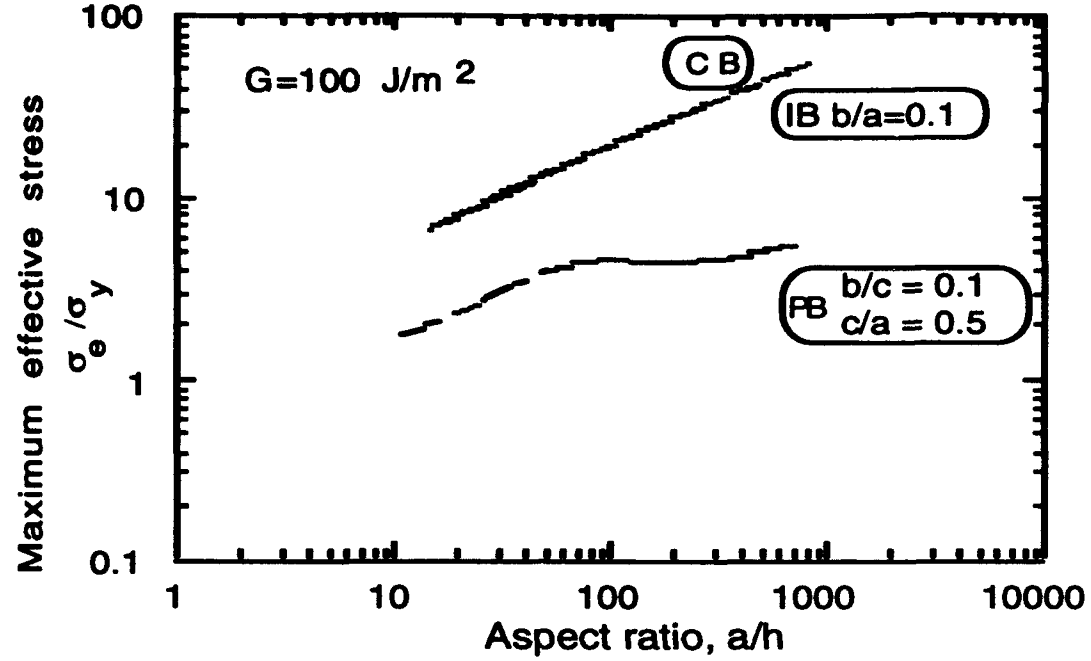

Figure 7. Maximum von Mises effective stresses in circular, island and peninsula blister specimens.

Large stresses very close to the delamination front do not pose much of a problem either in conducting tests or extracting linearly elastic fracture mechanics parameters. It is when the extent of yielding is large with respect to characteristic specimen dimensions, e.g., delaminating layer thickness, *h*, that interpretation of results becomes more complicated. With this in mind, the radial distribution of von Mises effective stresses at the critical pressure level for *100 J/m*^{2} were plotted in Figures 8 and 9 for the circular and island blisters, respectively. The longitudinal and spanwise effective stress distributions in the peninsula blister appear in Figures 10 and 11, respectively. In each case, the three subfigures a, b and c depict the stress distributions at the mid-thickness ($z/h = 0$) and the bottom and top surfaces ($z/h = \pm 0.5$) of the delaminating layer for $a/h = 10$, *100*, ana *500*, respectively capturing plate, transition and membrane behavior.

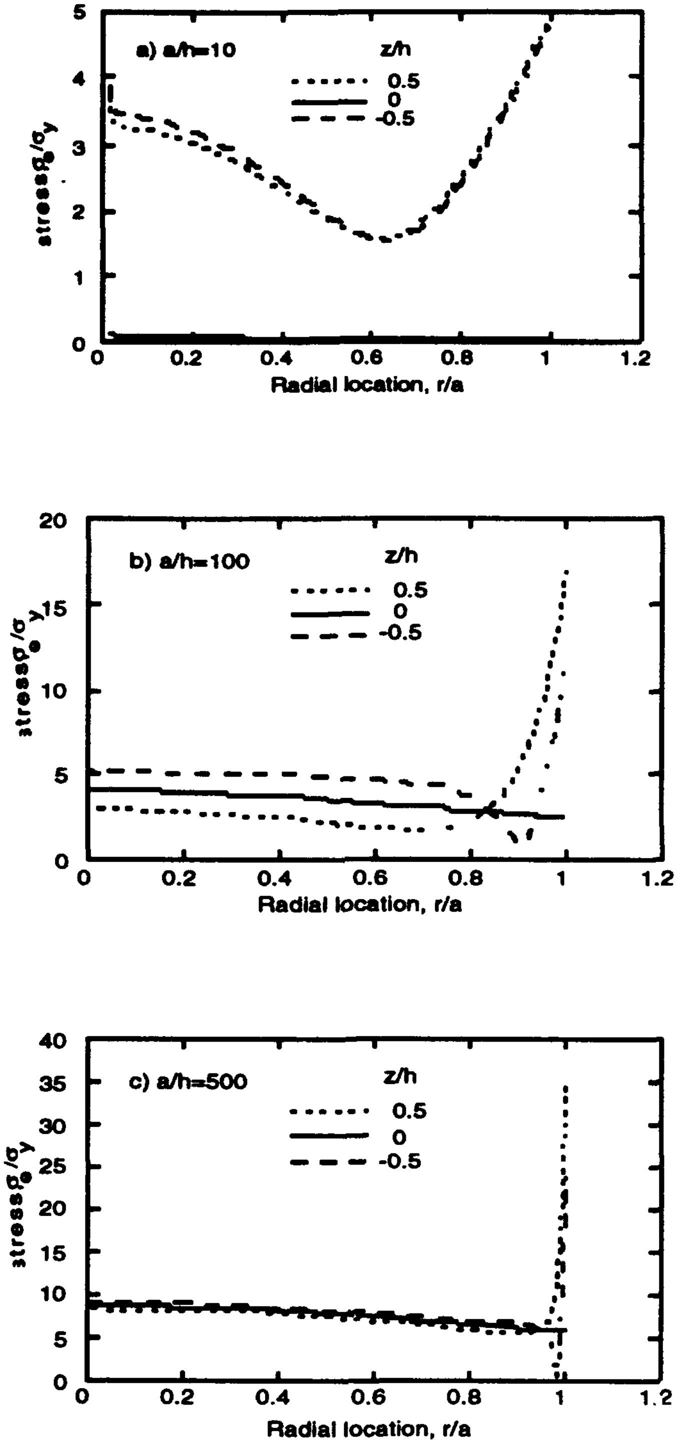

Figure 8. Von Mises effective stress distribution in (a) plate, (b) transition and (c) membrane configurations of the circular blister.

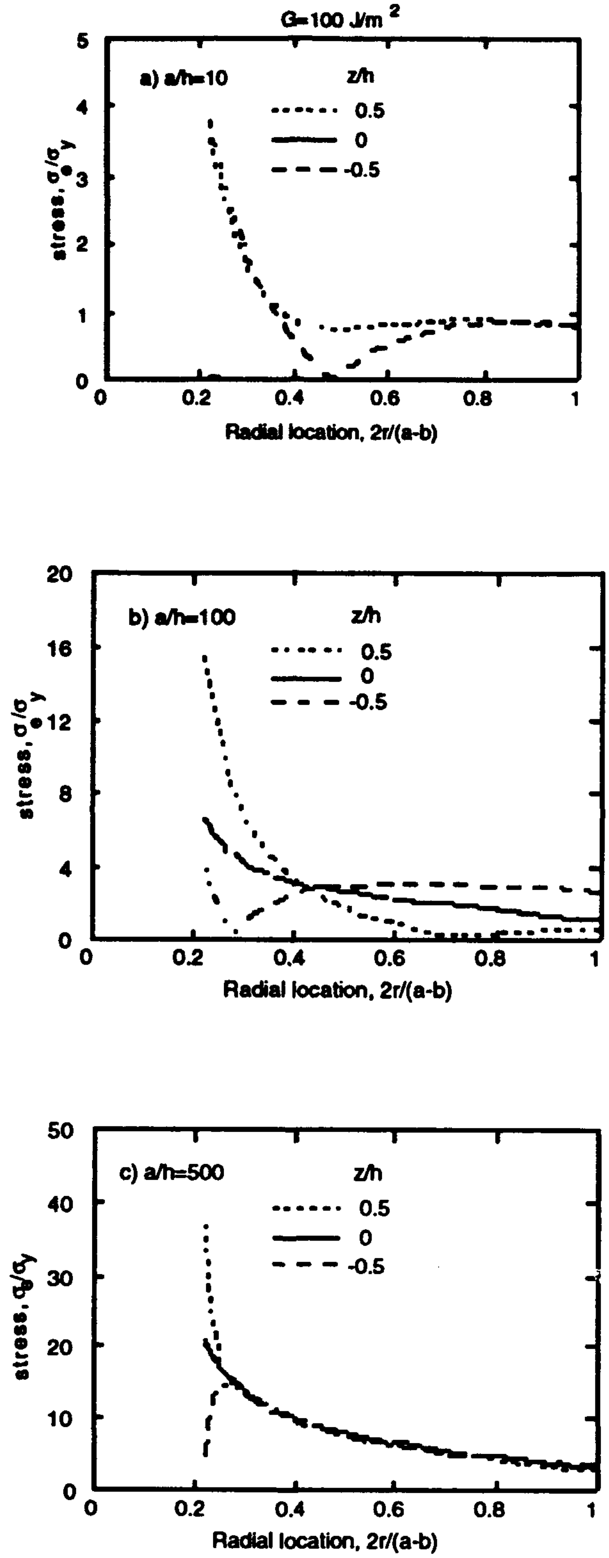

Figure 9. Von Mises effective stress distribution in (a) plate, (b) transition and (c) membrane configurations of the island blister.

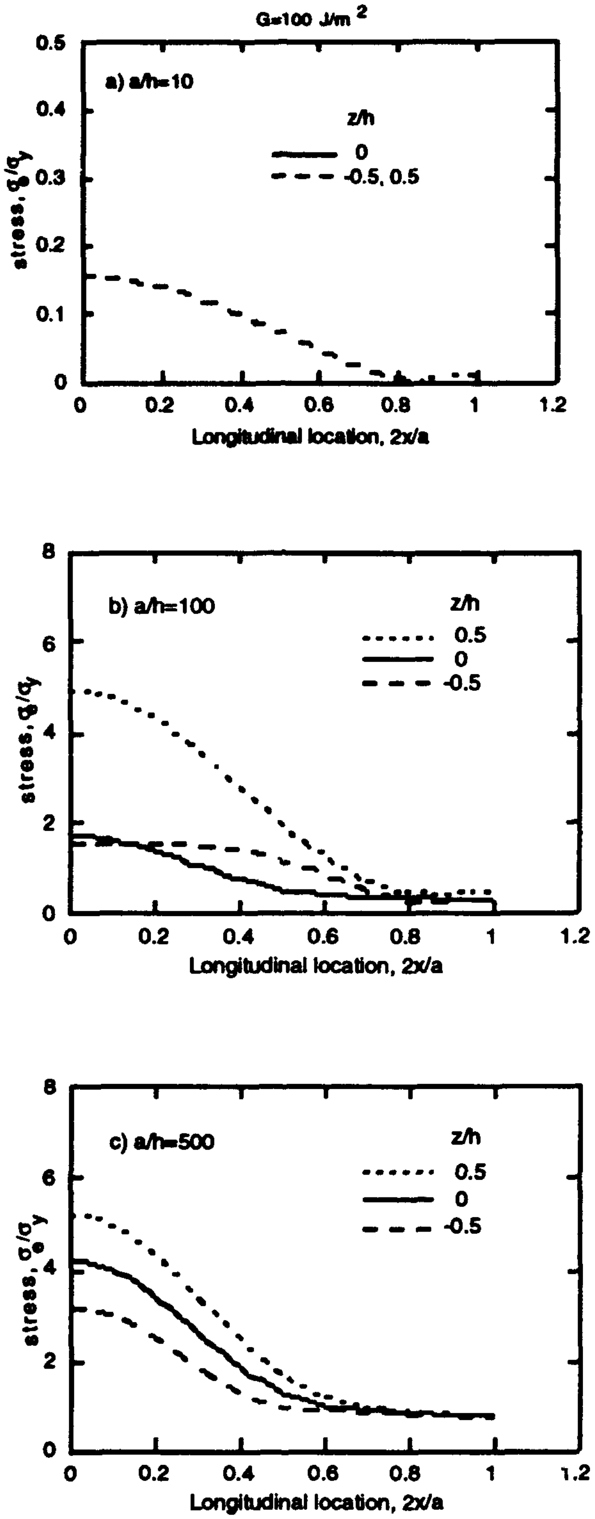

Figure 10. Longitudinal von Mises effective stress distribution in (a) plate, (b) transition and (c) membrane configurations of the peninsula blister.

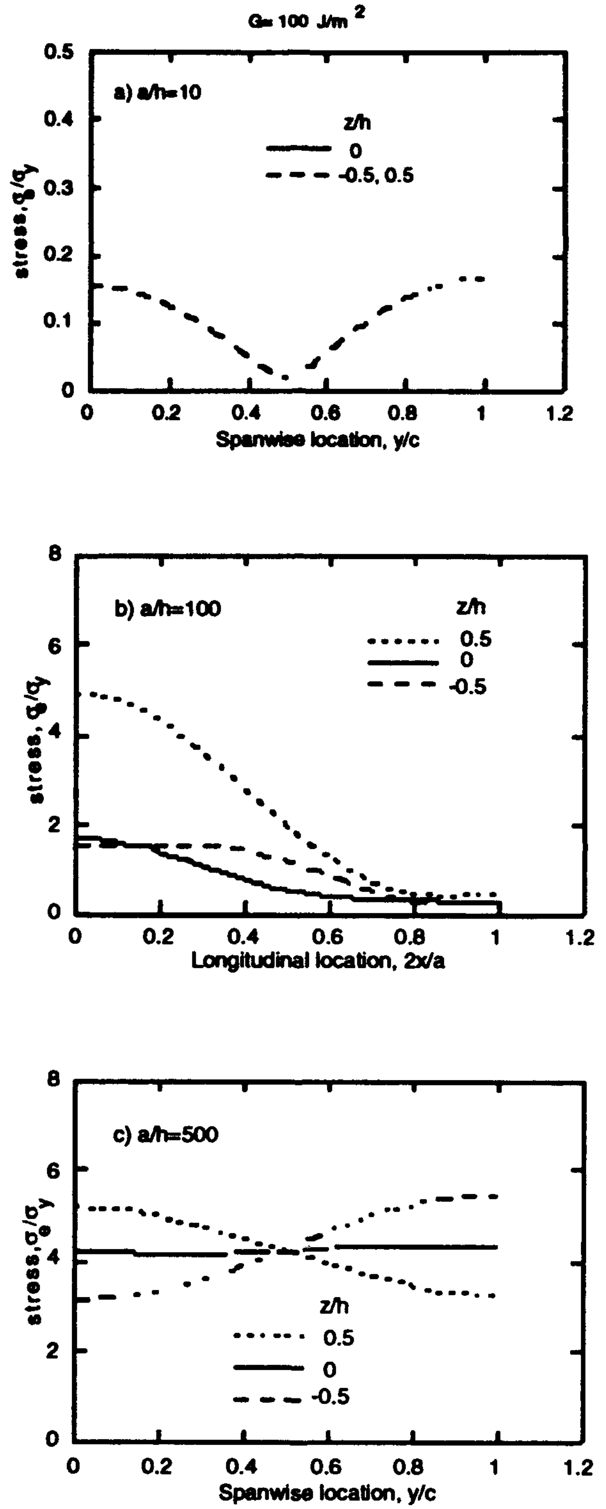

Figure 11. Spanwise von Mises effective stress distribution in (a) plate, (b) transition and (c) membrane configurations of the peninsula blister.

Looking at the circular blister and the *a/h = 100* configuration, which is most representative of the film thicknesses and delamination lengths obtained from standard microelectronics processing procedures we see (Figure 8b) that along all three surfaces the stresses were nearly constant near the center of the blister (*r/a = 0*) and grew in magnitude as the delamination front was approached. The degree of yielding was complete along all surfaces, with the exception of a small region near the minimum value for *z/h = -0.5*, the top of the delaminating layer. Thus the amount of yielding in a circular blister with *a/h = 100* at critical pressure for $G = 100\ J/m^2$ is extensive, and, if not properly accounted for, would give rise to a substantial overestimate of fracture toughness. The stress distributions for *a/h = 10* and *500* are shown in Figures 8a and c, respectively. Although the membrane stress *(z/h = 0)* drops to zero for the plate configuration *(a/h = 10)*, complete yielding occurred along the top and bottom surfaces. These large amounts of yielding, even in the plate configuration, help explain why higher values of interfacial toughnesses were obtained with circular blister specimens[35,43] and the propensity of delaminating circular blister films to burst.[30]

In analyzing the island blister specimen, we examined a number of values of the ratio of initial island radius to outer delamination radius, but present only the results for one case: *b/a = 0.1*. The extent of yielding in the island blister configuration for $G = 100\ J/m^2$ and *a/h = 10*, *100* and *500* can be seen in Figures 9a, b and c, respectively. The value *r = 1* corresponds to the center of the annulus. The highest stress magnitudes occurred near the island perimeter (*r = 0.22*). The extent of yielding was greatest for the membrane (*a/h = 500*), where there was complete yielding. For the transition case (*a/h = 100*), there was complete yielding of the delamination along the midplane of the film and a small elastic region near the minimum that arose along the top surface. There was an elastic response over about 50% of the bottom surface of the delaminating layer. Yielding in the plate configuration (*a/h = 10*) was less severe and only occupied about 10% of the exterior surfaces. The lower stress levels in the island blister support the observation[30,31] that delaminating films that had been bursting in the circular blister no longer did so when the island blister was used, even though residual stresses were present.

The distribution of von Mises effective stress levels in the peninsula blister along *y = 0* is shown in Figures 10a, b and c. The stress along the mid-thickness decreased with increasing aspect ratio to zero for *a/h = 10*. For the membrane and transition configurations, the membrane stress was the highest at *x = 0* and yielding occurred over 55 and 30%, respectively, of the delamination length. For *a/h = 500*, the stresses along the top and bottom surfaces exceeded the yield strength over 50 and 60% of the delamination length, respectively. Although the stress levels along the mid-thickness dropped for *a/h = 100* (Figure 10b), there was redistribution of the stresses along the top and bottom surfaces that gave rise to slightly larger amounts of yielding. However, the plate configuration (*a/h = 10*) gave rise to completely elastic behavior (Figure 10a), making it very suitable for fracture toughness testing. The pattern of extensive yielding for *a/h = 500* and *100* and no yielding for *a/h = 10* was repeated for the spanwise distributions (Figure 11). A more complete picture of the distribution of yielding along the bottom of the delaminating layer is given in the contour plots in Figures 12a and b for *a/h* = *10* and *100*, respectively. The area being examined is the quadrant $0 \leq x \leq a/2$ and $-c \leq y \leq 0$. While it is clear that no yielding occurred for the plate configuration ($a/h = 10$), there was a substantial amount of yielding for $a/h = 100$. The stresses were concentrated in the middle of the delamination and exceeded the yield strength in an elliptical region with semi major and minor axes that were, respectively, about 80% of the delamination length and 70% of the span of the delamination. At this point it should be remembered that this was a two-dimensional analysis, with all four boundaries being fully clamped. A full three-dimensional analysis would be required to completely capture the partial clamping of the boundary $x = a$, for $0 \leq |y| \leq b$, which would undoubtedly raise the stresses locally but not raise the overall extent of yielding very much.

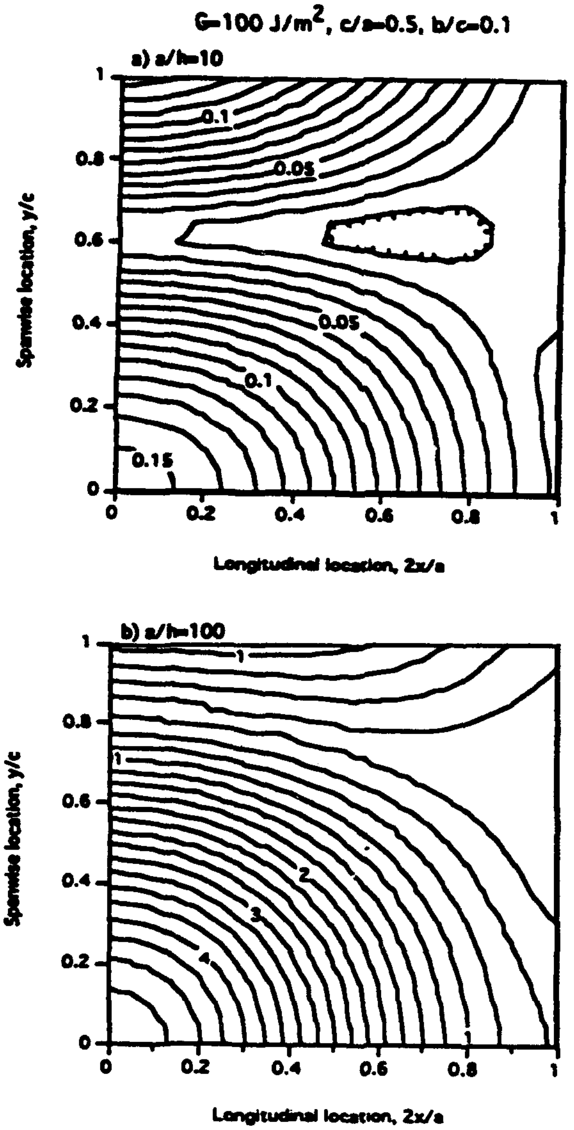

Figure 12. Von Mises effective stress contours in peninsula blisters with aspect ratios (a) a/h = 10, and (b) a/h = 100.

Unfortunately, it is not simple to take advantage of the lack of large scale yielding offered by the $a/h = 10$ configuration because of limitations in the thickness of the deposited copper layer. As discussed below, in our test specimens, the copper layer is first vacuum deposited onto the polyimide to a thickness of 0.1μm and then thickened to at most 1μm by electrodeposition of copper or gold. Any further thickness augmentation by electroplating causes residual stresses of sufficiently high magnitude that spontaneous delamination can occur. An alternative scheme for preventing excessive yielding was therefore considered in the form of a stronger, slightly more compliant layer bonded to a 1μm copper layer with epoxy, which can be spincoated to a thickness of about 2-10μm. Mica was considered as an example of a potential top layer with a thickness of 20-30μm. At an $a/h = 100$, this would allow an initial crack length of $a = 2mm$ to be used. Since the mica was so much thicker than the copper/epoxy combination, the configuration was first analyzed as a homogeneous mica layer to determine critical pressures, etc. for $G = 100 J/m^2$. The strains were then used to determine the stresses in each layer using the properties listed in Table 2 and a laminated plate theory that was suitably modified for the von Karman kinematics. The resulting von Mises effective stresses at the bottom of each layer are shown in Figure 13, where the stress for each layer was normalized by the corresponding yield stress (failure stress for the mica), listed in Table 2. As might be expected, the largest stress levels were in the copper. However, the stress levels never exceeded 50% of the yield stress, even though the aspect ratio was 100, which had caused yielding in the homogeneous case. Consideration was also given to using the mica layer for circular and island blisters. Effective stress levels in the copper were slightly above the yield strength in the circular blister and the critical pressure level was much higher. The critical stresses and pressure levels in the island blister were closer to the levels encountered in the peninsula blister, but it is not a constant (steady state) energy release rate specimen. Thus the mica layer can indeed function as a yielding inhibitor and increase the potential for thin film delamination tests to be conducted on the basis of linear elastic fracture mechanics.

Table 2. Mechanical Properties of Delaminating Layers

Material	Young's Modulus E, (10^6psi / GPa)	Poisson's Ratio ν	Yield Strength σ_y, (ksi / MPa)
Copper	16 / 110.2	0.30	10 / 68.9
Epoxy	0.5 / 3.5	0.40	2 / 13.8
Mica	10 / 68.9	0.30	50 / 344.5 *

* Failure strength

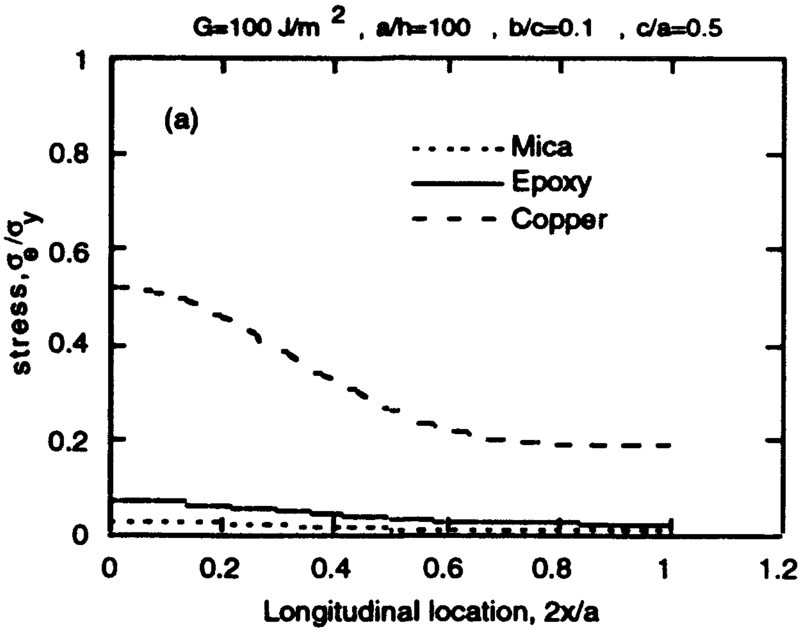

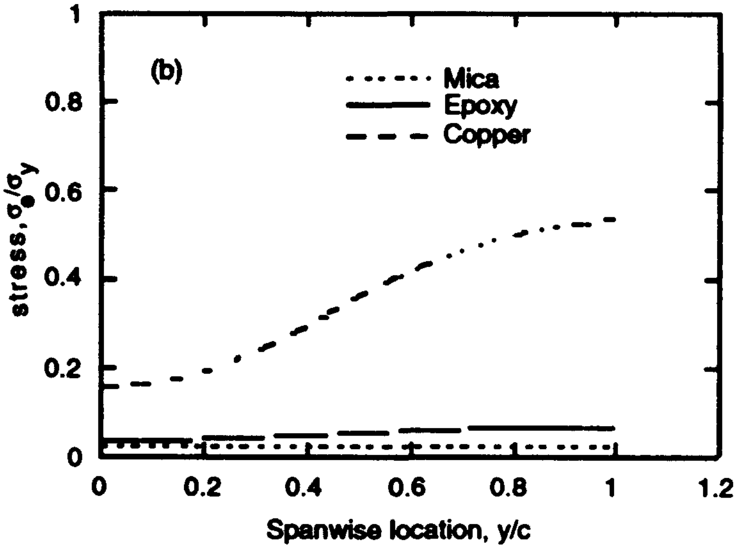

Figure 13. Longitudinal and spanwise distributions of von Mises effective stresses in a composite peninsula blister.

FABRICATION PROCEDURE

The requirements identified by the stress analysis for no inelastic deformation present a challenge for fabrication. Peninsula blister specimens previously have been fabricated on a much larger scale by millling aluminum plate and bonding a membrane using adhesive.[34] Such a procedure is not compatible with our system and was not intended to eliminate inelastic deformation, but rather to reduce the pressure required for crack propogation and to minimize the chance of membrane rupture. Although island blister specimens have been fabricated by standard electronic material lithography previously,[30,31] this structure is less complicated than the peninsula blister and again the structure was not designed to eliminate inelastic deformation and, hence, did not have the design constraints developed here. Increasing the overlayer thickness was one challenge that has already been discussed. Another involved development of etching procedures that would etch away the silicon substrate and then the polyimide from the "ocean" without attacking the copper or promoting delaminations at the copper/polyimide or polyimide/substrate interfaces. Additionally, the etched walls had to be steep so that the back side of the peninsula (away from the polyimide) had sufficient area to be reliably bonded to the backing wafer to act as a rigid platform for crack front propagation.

By iteration and compromise between the analyst and the production engineer, we have developed a workable fabrication procedure that results in an analysible structure that can be correlated to the XPS measurements discussed in the next section. Those steps requiring additional explanation are discussed following the listing:

- Spin coat the poly(amide acid) precursor onto 3-in. silicon wafer.
- Cure the polyimide at 140°C for 0.5 hours, cool to room temperature, and further cure at 300°C for 1 hour.
- Evaporate ~150 nm copper onto the polyimide using the electron beam evaporator in the preparation chamber of the XPS system.
- Electroplate ~1 μm gold onto copper surface.
- Spin coat ≤10 μm room-temperature curing epoxy onto gold surface.
- Bond a 20-30 μm mica wafer to the metallized polyimide.
- Apply photoresist to back side of wafer and expose with appropriate mask.
- Etch silicon in the "ocean" area using silicon tetrachloride in a reactive ion etch (RIE) system.
- Etch the polyimide in the "ocean" area using oxygen in the RIE system.
- Etch a 2-mm hole through a second wafer using RIE.
- Spin coat the room-temperature curing epoxy onto the second wafer and bond to first wafer.

The first three steps are identical to those performed during XPS measurements to obtain the interphasal chemistry. This equivalency is critical to make the correlation between the chemistry and fracture toughness. The only difference is that the evaporation is not done in steps as it is for XPS, but done continuously. A similar evaporation rate is used in both cases.

Approximately 1μm additional gold is electroplated to increase the rigidity and strength of the overlayer. It has the added benefit of increasing the robustness during fabrication. To further strengthen the overlayer to prevent plastic deformation during testing and to provide the desired *a/h* ratio, a 20-30 µm mica layer is glued to the copper with a spun-coated, low-viscosity, room-temperature curing epoxy.

Four blister specimens are produced on each wafer to provide redundancy and to increase yield. The size and aspect ratio of the peninsula together with the thickness of the wafer require steep walls to minimize undercutting and weakening of the peninsula and to allow anchoring of the peninsula to the second wafer. This is acheived by etching of Si and polyimide in an RIE system using silicon tetrachloride and oxygen, respectively.

The four inlet holes that are etched in the second silicon wafer (also via RIE) are aligned with the "oceans" of the first wafer. This wafer is then glued to the back of the first wafer to enclose the pressurization volume and allow pressurization to be performed.

INTERPHASAL CHEMISTRY

Carbon and oxygen spectra for the four clean polyimides are shown in Figure 14 and binding energies for the different peaks are given in Table 3. The different concentrations of carbonyl and ether moieties are evident. For PMDA-ODA, the spectra and binding energies agree well with previously reported results.[2] The splitting of the dianhydride and diamine aromatic carbons are also evident. Model compound analysis[48,49] has previously indicated that at least three carbonyl groups need to be attached to a ring for this splitting to be observed. Our results show that each carbonyl group, up to three, cause a shift of ~0.3 eV: The DABP with one carbonyl moiety has a C 1s peak shifted by 0.3 eV relative to the other diamine components with no carbonyl groups while the ODPA with two carbonyl moieties has a peak shifted by 0.7 eV. No additional shift is seen in going from three to four carbonyl groups; both PMDA and BTDA have a shift of 1.0 eV relative to the aromatic structures without carbonyls.

Table 3. Binding Energies for Clean Polyimides (eV)

polyimide	C-O-C	C=O	N	C=O	C-O	N-C, C-C dianhydride	C-C diamine
PMDA-PDA	-	532.3	400.8	288.9	-	286.0	285.0
BTDA-DABP	-	532.3	401.0	289.1	-	286.0	285.3
ODPA-ODA	533.6	532.3	400.8	288.9	286.8	285.7	285.0
PMDA-ODA	533.6	532.3	400.9	289.0	286.8	286.1	285.1

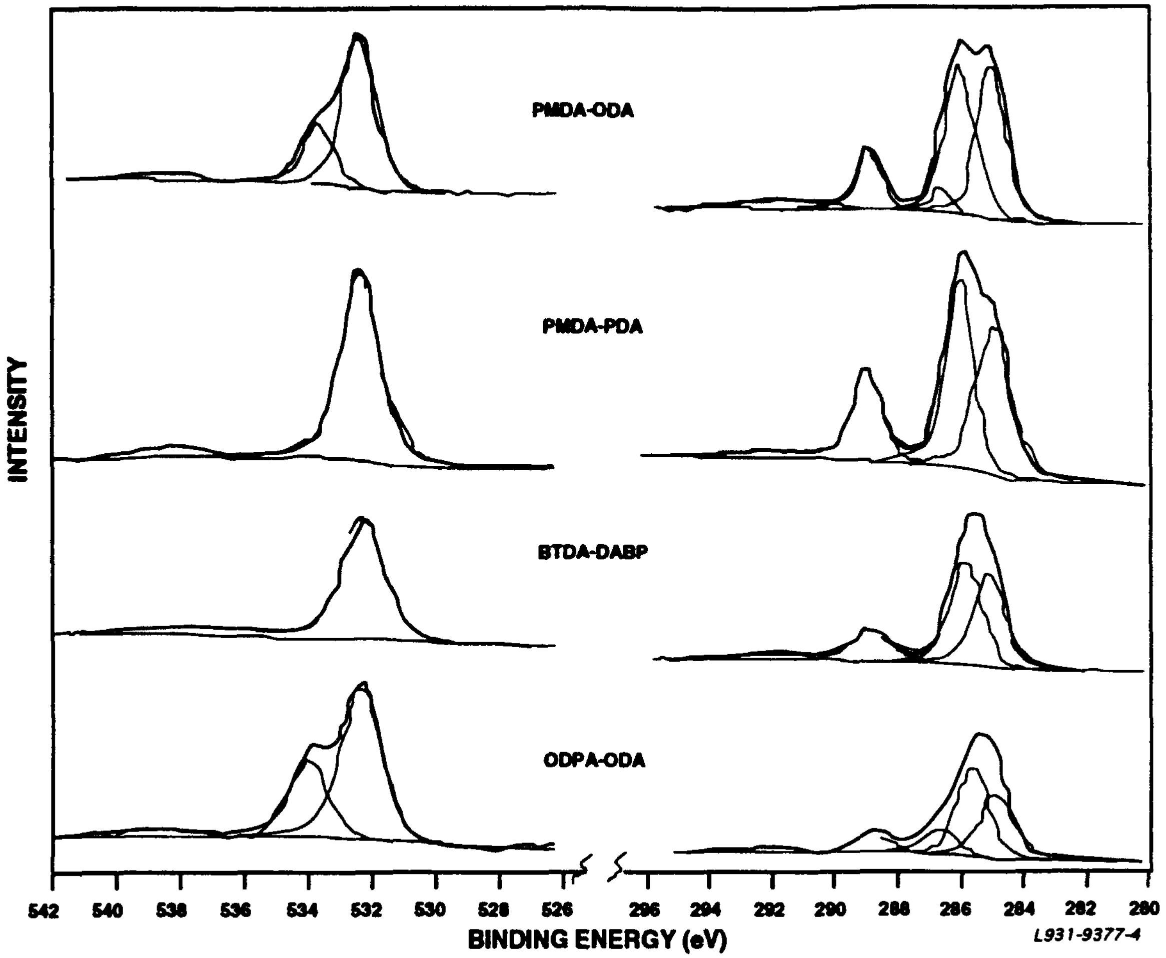

Figure 14. Carbon and oxygen 1s spectra for clean polyimides.

Representative spectra of PMDA-PDA, the simplest polyimide examined, following deposition are shown in Figure 15. One of the most notable features is the appearance of an ether-like functionality in both the carbon and oxygen spectra at moderate to high coverages (>1 nm Cu). A similar emergence of a carbon ether-like moiety is also observed for BTDA-DABP, the other polyimide without ether linkages in its structure.

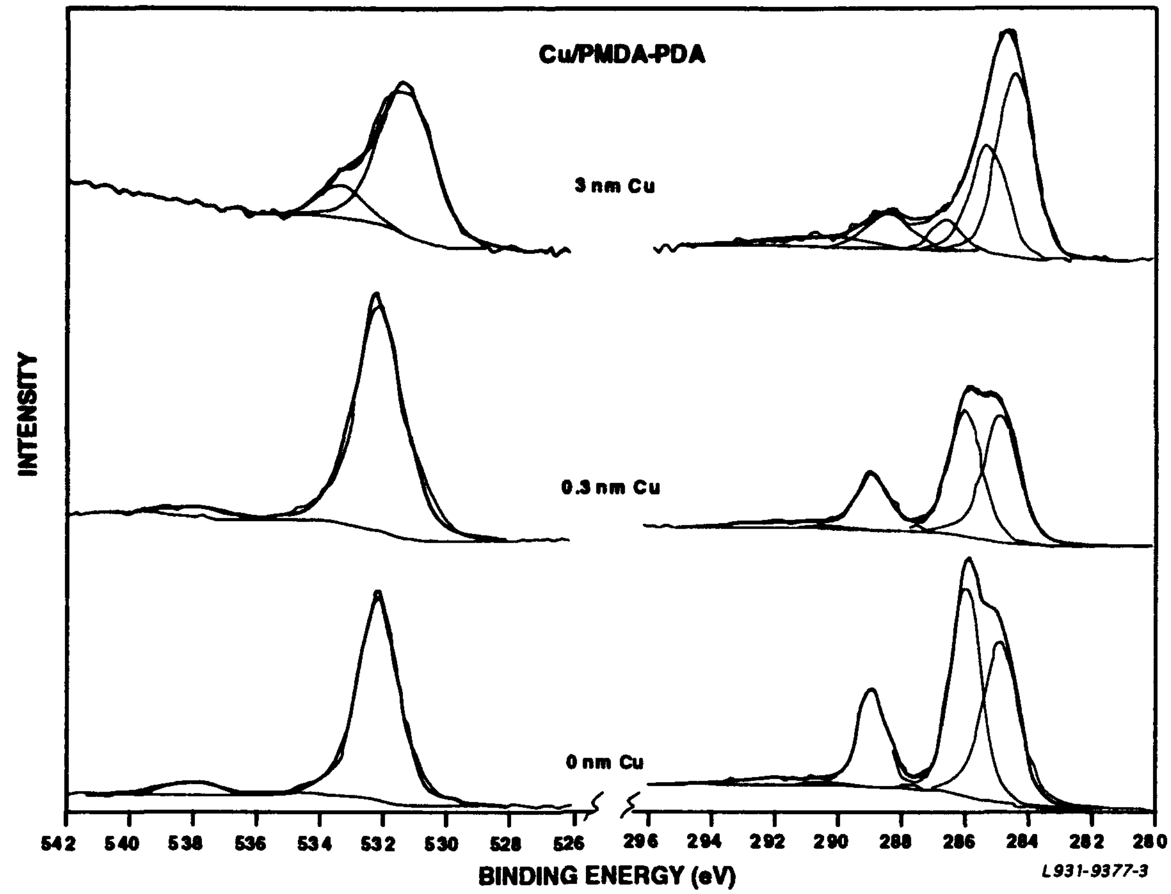

Figure 15. Carbon and oxygen 1s spectra of PMDA-PDA for a clean substrate and after deposition of approximately 0.3 and 3 nm of copper.

Normalized concentrations of oxygen and carbon exhibiting carbonyl and ether bonding as a function of copper concentration are shown for the four polyimides in Figures 16 and 17. The carbonyl oxygen concentration decreases linearly with increasing copper concentration with a slope of -1 as expected for a simple attenuation behavior. In contrast, the ether oxygen value for PMDA-ODA and ODPA-ODA, the polyimides with initial ether linkages, falls off more rapidly initially (up to 30% Cu) and then decreases much more slowly. For PMDA-PDA, an ether oxygen peak is first detected at 40% Cu and slowly increases with increasing copper coverage. No such peak is detected for BTDA-DABP.

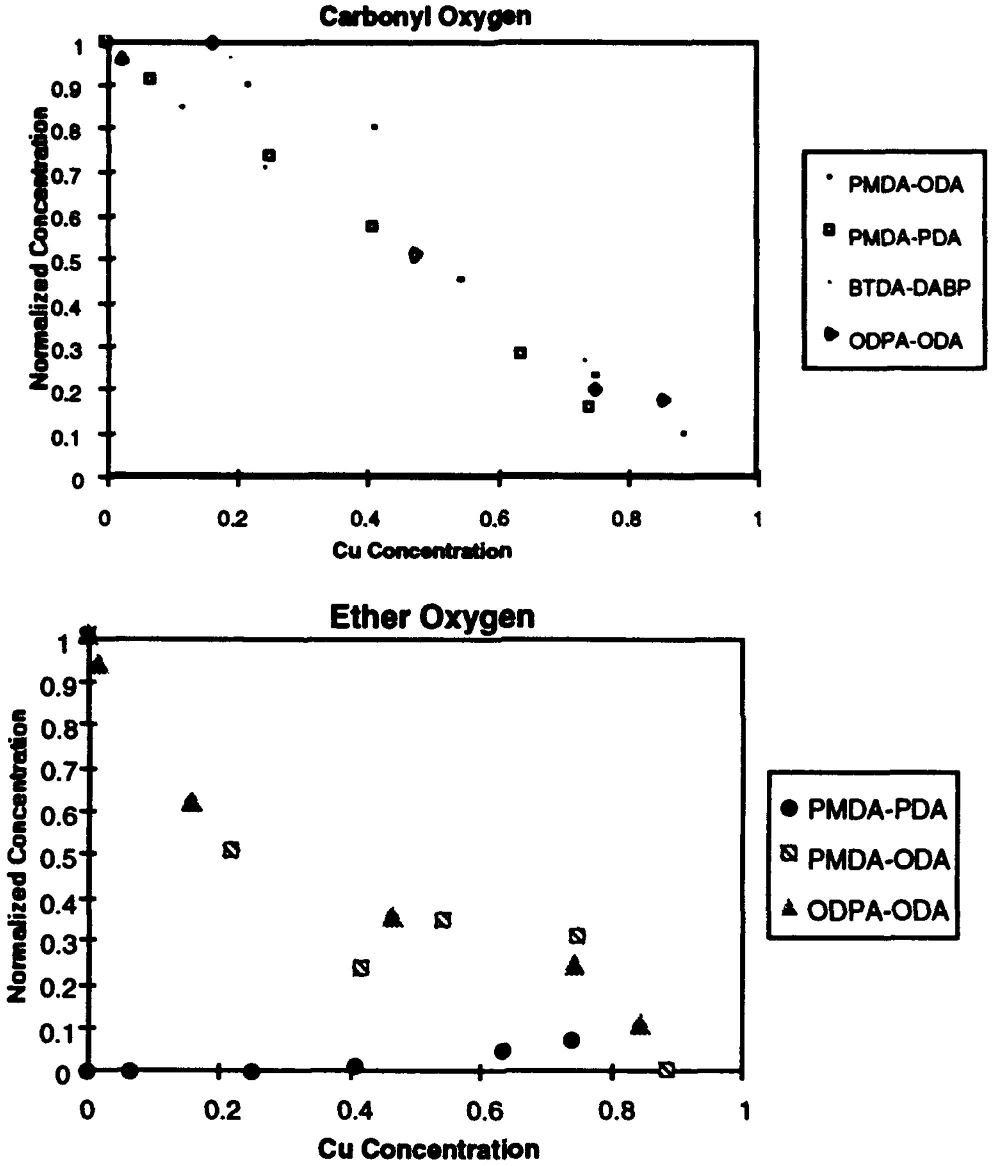

Figure 16. Normalized concentrations of carbonyl and ether oxygen as a function of copper concentration.

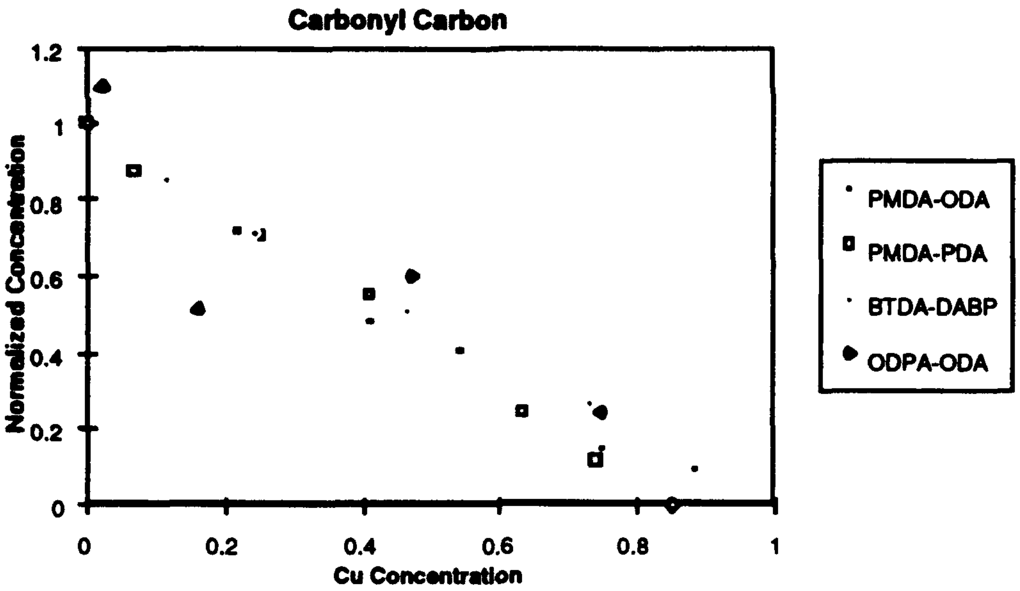

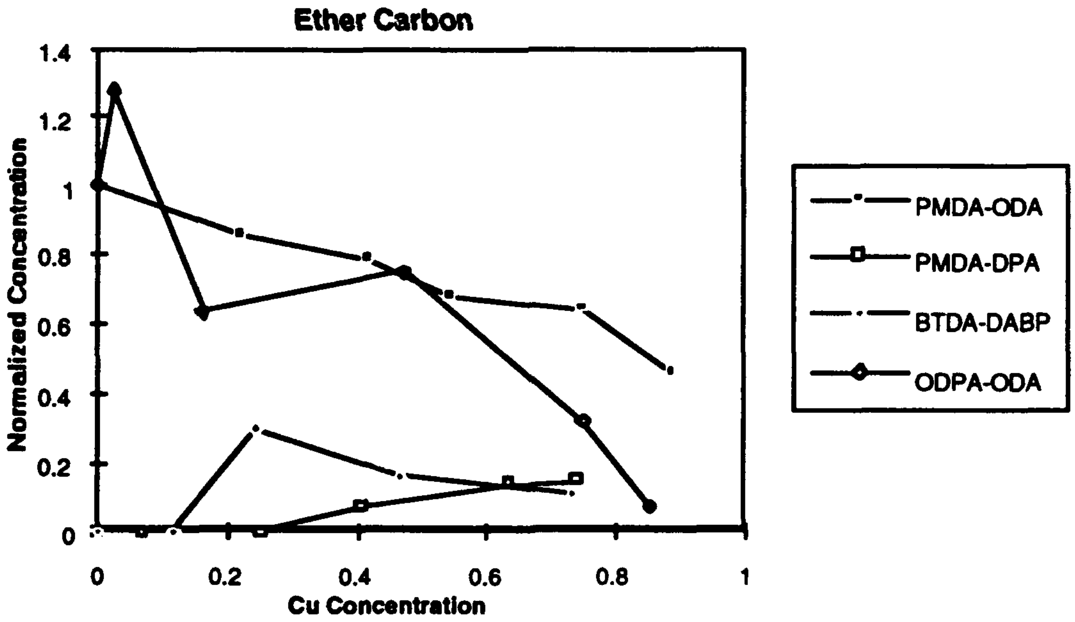

Figure 17. Normalized concentrations of carbonyl and ether carbon as a function of copper concentration.

The carbonyl carbon concentration also decreases linearly with increasing copper concentration, but with a slope slightly less than -1. This more rapid decrease in signal is a result of either a greater attenuation due to a reaction with this moiety or preferential adsorption or a small error in the relative sensitivity factors of carbon and copper. At this point, we cannot eliminate any of these possibilities although observation that the average aromatic carbon signals do not decrease more rapidly than expected from attenuation considerations suggests that the small difference in carbonyl fall off may be real and not a sensitivity factor artifact. The ether carbon concentration exhibits considerably more scatter reflecting the greater uncertainty in curve fitting this small peak. The PMDA-ODA signal clearly decreases much more slowly than expected from attenuation considerations while the fall off of the ODPA-ODA peak cannot be distinguished from a simple attenuation. Ether carbon peaks appear in both BTDA-DABP and PMDA-PDA midway through the deposition sequence and persist until the end (10 nm Cu) although with different trends.

The aromatic carbon species tend to follow the expected attenuation. The only exceptions are the diamine signals from PMDA-ODA and PMDA-PDA (Figure 15) which decrease more slowly at low copper coverages. One possible explanation of this slower decrease would be a greater attraction of the copper to the PMDA component which is the most compact dianhydride studied.

The full widths at half maximum (FWHM) of the various peaks can also contribute to the understanding of interfacial reactions. The Cu $2p_{3/2}$ peak is relatively broad at the first coverages, but narrows with increasing coverage until sufficient copper is present to form a metallic overlayer (Figure 18). The consistency of the FWHM at coverages greater than 25% Cu suggests that whatever interactions occur at the interface do not involve significant charge transfer from the copper and its metallic state is maintained.

The two oxygen peaks behave very differently as shown in Figure 19. The ether oxygen changes very little over the course of the depositions with perhaps a slight decrease and then increase. In contrast, the carbonyl peaks steadily broaden until ~40% Cu, remain steady until ~60% Cu, and then narrow until the end of the experiments.

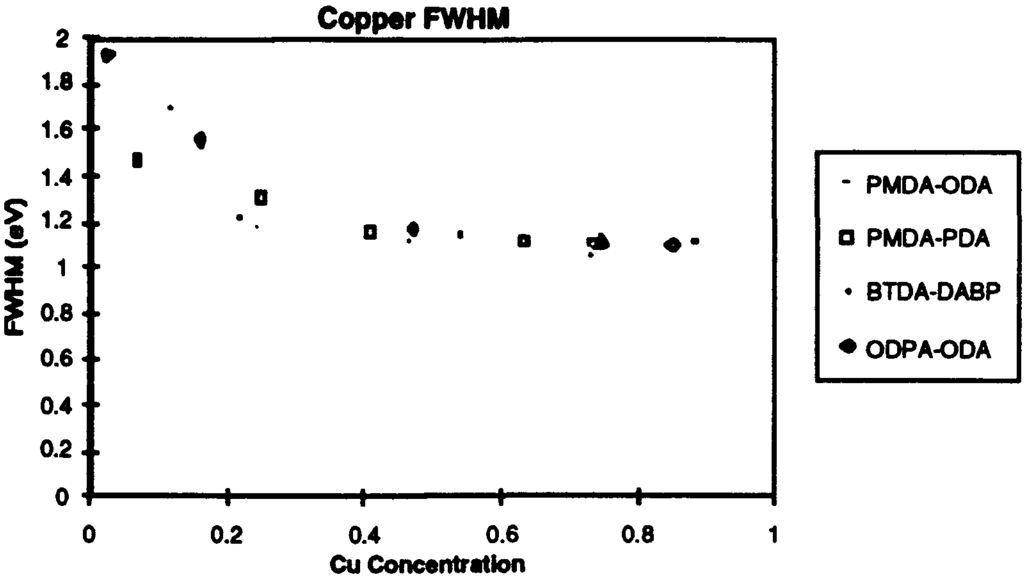

Figure 18. FWHM of Cu $2p_{3/2}$ peak as a function of copper concentration.

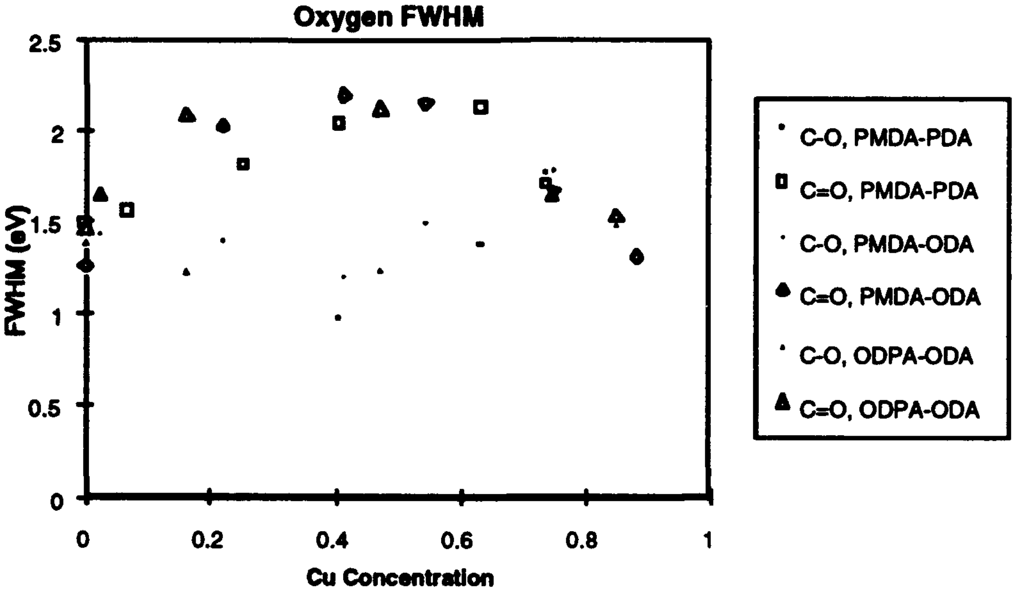

Figure 19. FWHM of O 1s carbonyl and ether peaks as a function of copper concentration.

The carbonyl carbon peaks show a steady rise during the entire deposition sequence (Figure 20). The increased width of the BTDA-DABP peak reflects the two nonequivalent carbonyl sites (four on the dianhydride and one on the diamine) and demonstrates the sensitivity of the FWHM to different chemical environments. Because of the greater uncertainty in curve fitting the small ether carbon peak, it is less reliable as a probe of chemical state. Of the two polyimides containing ether linkages, the width of the ODPA-ODA is much greater because of the two nonequivalent sites on the dianhydride and diamine components. The PMDA-ODA peak steadily broadens during deposition until its width is close to that of ODPA-ODA. Again the two emergent ether peaks (PMDA-PDA and BTDA-DABP) show different trends with increasing copper coverage. The reason for this different behavior is not understood.

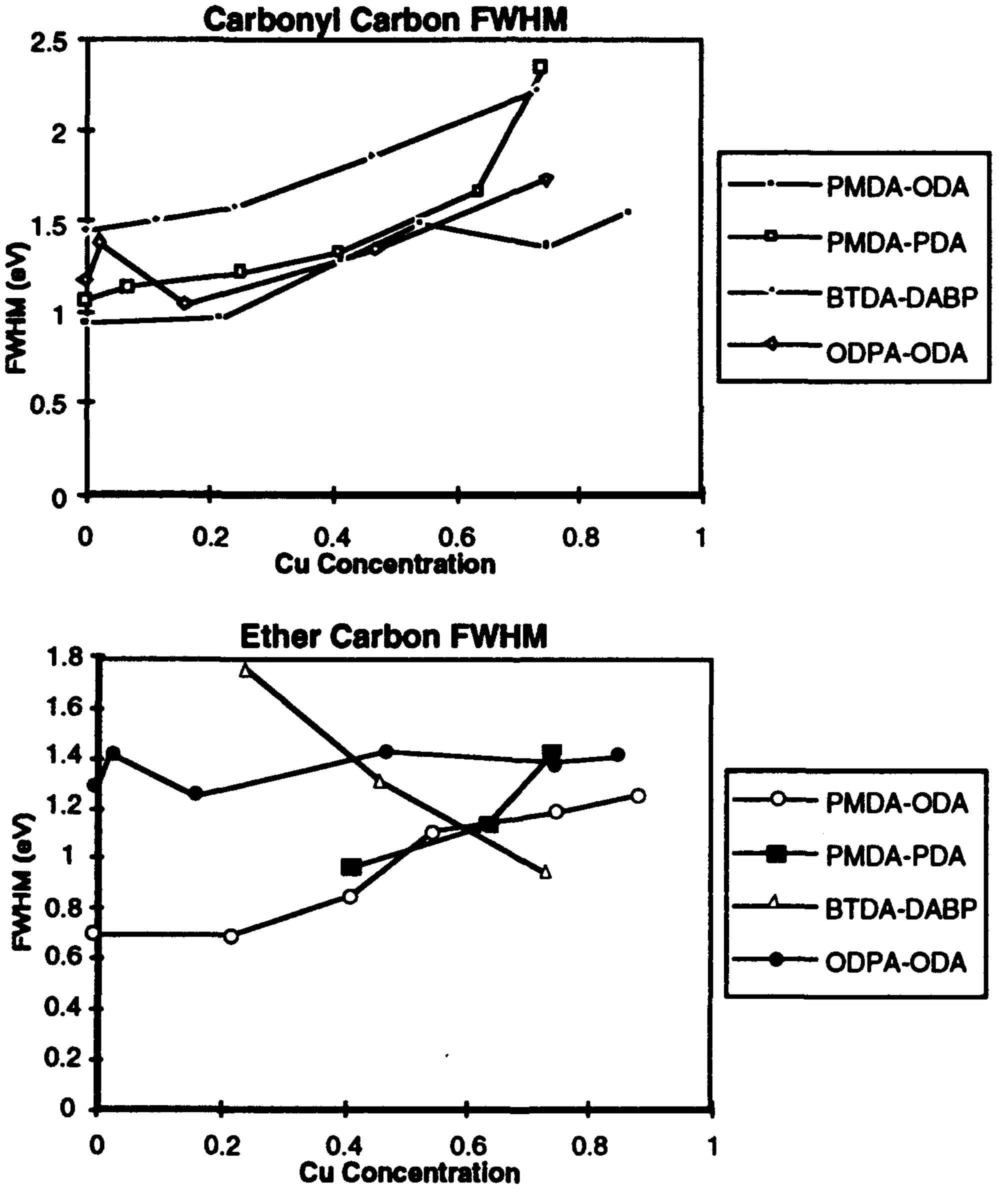

Figure 20. FWHM of C 1s carbonyl and ether peaks as a function of copper concentration.

In contrast to the behavior of the oxygen peaks and carbon peaks bonded to oxygen, the aromatic carbon peaks maintain nearly constant widths. The FHWMs for all coverages and all polyimides are within or close to a band from 1.1-1.3 eV. The same consistency is also observed for the nitrogen peak until, at high coverages, the reduced signal-to-noise increases the scatter.

Much of these data can be summarized by representation in the surface behavior diagram (SBD) of Figure 21. SBDs have been used to trace the evolution of the surface composition during a variety of reactions with the environmentand as a function of depth into the material.[55-58] Often, the SBD representation allows insights not readily available from more conventional analyses. In this case, only the carbon chemistry is plotted onto the SBD to elucidate its interfacial reactions; the basis species that occupy the vertices of the SBD are the carbonyl, ether, and aromatic carbons. (The aromatic carbon signal is the sum of the dianhydride and diamine values, which also include the carbon-nitrogen bonding.) Here we show the evolution of the carbon chemistry for PMDA-PDA and PMDA-ODA with copper coverage as the independent parameter. The data show a steady evolution along a horizontal line parallel to the carbonyl-ether axis for both polyimides, except for the 88% Cu point of PMDA-ODA which deviates downward. That horizontal path is indicative of a partial replacement of carbonyl functionality with ether-like functionality. The replacement is most evident with the PMDA-PDA because there are no initial ether moieties to mask the emergent ether-like moieties. By 75% Cu coverage, the carbon chemistry of the two polyimides is essentially identical.

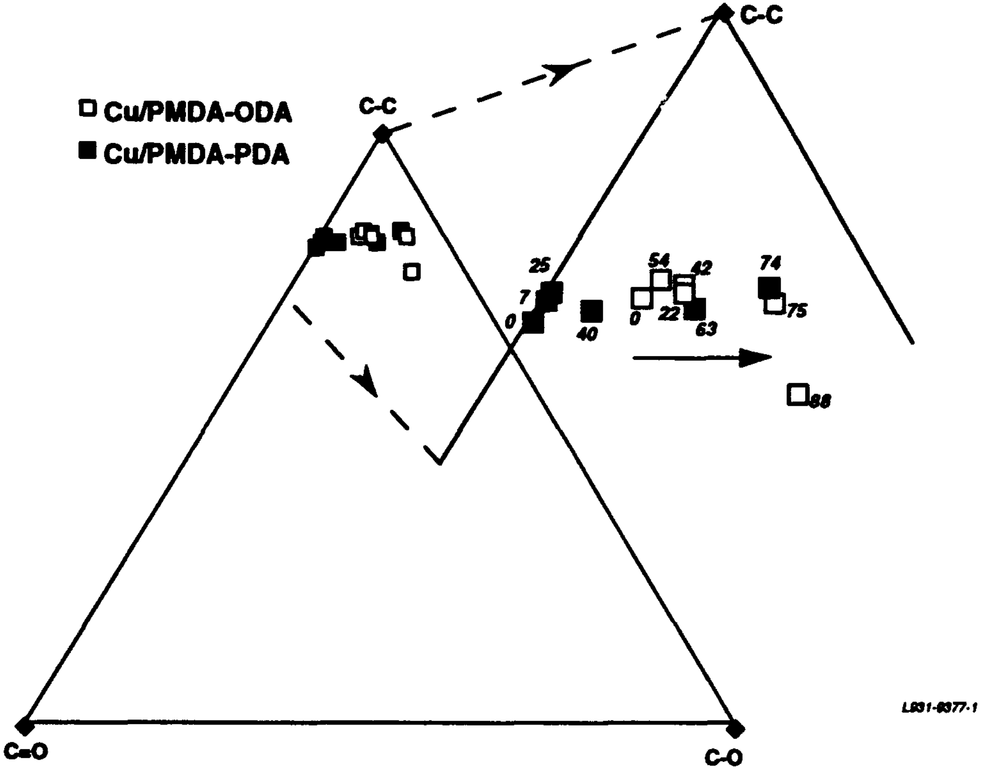

Figure 21. Surface behavior diagram tracing the evolution of the carbon chemistry as a function of copper concentration for PMDA-PDA and PMDA-ODA. The numbers beside each peak represent the atomic concentration of copper.

The precise form of this ether-like functionality is unclear. The leveling off of the PMDA-ODA and ODPA-ODA ether oxygen signal beginning at ~30% Cu after an initial rapid decrease (Figure 16) corresponds to the point at which the emergent ether-like carbon signals are first detected for BTDA-DABP and PMDA-PDA and the emergent ether-like oxygen signal is first detected for PMDA-PDA. Nonetheless, the FWHM of the Cu peak remains narrow in this regime arguing against a covalent Cu-O-C bond. Rather, copper appears to remain metallic while inducing charge transfer from the carbonyl groups equivalent to the formation of an ether group.

The observation that copper reacts only weakly with a polyimide substrate at room temperature is well established in the literature.[11-15] The site of the interaction with unreactive metals, however, is less certain with carbonyl[11] and ether[14] moieties being proposed along with a general, non-specific reaction site.[3,12,15,16] Our data are strong evidence that copper interacts with the carbonyl moieties and at least partially reduces the carbon to form ether-like functionalities. This reaction is similar to that observed initially for reactive metals, but requires much more copper. The comparison of the interphase chemistry with interphase mechanical properties will further elucidate the bonding sites and mechanisms.

SUMMARY AND CONCLUSIONS

Although the range of specimen configurations that was analyzed here was greater and the manner in which they were analyzed was more consistent, the conclusions of previous analyses, namely that the peninsula blister specimen provides the highest energy release rates, still stand. However, the new insight provided by the present analysis was that the amount of yielding in all specimens, and particularly the circular blister, can be substantial, especially for aspect ratios and toughness values that occur in multilayered microelectronics structures. The only configuration with a homogeneous delaminating layer that did not suffer any yielding was the relatively thick ($a/h = 10$) peninsula blister. The addition of a thicker, higher strength layer extended the range of aspect ratios over which linear elastic fracture mechanics could potentially be applied.

The interactions with deposited copper overlayers and various polyimide substrates have been investigated by monochromatized XPS. The emergence of ether-like functionalities on polyimides without innate ether groups and a broadening of the carbon carbonyl peak indicate a copper-induced reduction of some of the carbonyl functionalities. The surface behavior diagram of the carbon chemistry confirms this scenario by indicating a partial replacement of the carbonyl groups by ether-like moieties.

ACKNOWLEDGMENTS

We would like to gratefully acknowledge the synthesis of the polyimides by T.L. St.Clair and C.I. Fay, valuable discussions with H.M. Clearfield, and technical assistance by C.R. Anderson and J.K. Whisnant. Thanks are also due to Ms. Jan Shrode (University of Texas) and Mrs. Dana Williams (Martin Marietta•Baltimore) for doing some of the word processing. This work was funded by ONR under contract N00014-C-92-0004.

REFERENCES

[1]J.W. Bartha, P.O. Hahn, and F. LeGoues, *J. Vac. Sci. Technol. A* **3**, 1390 (1985).

[2]F.S. Ohuchi and S.C. Freilich, *J. Vac. Sci. Technol. A* **4**, 1039 (1986).

[3]N.J. DiNardo, J.E. Demuth, and T.C. Clark, *J. Vac. Sci. Technol. A* **4**, 1050 (1986).

[4]J.G. Clabes, M.J. Goldberg, A, Viehbeck, and C.A. Kovac, *J. Vac. Sci. Technol. A* **6**, 985 (1988).

[5]M.J. Goldberg, J.G. Clabes, and C.A. Kovac, *J. Vac. Sci. Technol. A* **6**, 991 (1988).

[6]J.G. Clabes, *J. Vac. Sci. Technol. A* **6**, 2887 (1988).

[7]A. Selmani, *J. Vac. Sci. Technol. A* **8**, 123 (1990).

[8]A. Chenite, A. Selmani, B. Lamontagne, and A. Yelon, *J. Vac. Sci. Technol. A* **11**, 2411 (1993).

[9]Lj. Atanasoska, H.M. Meyer, III, S.G. Anderson, and J.H. Weaver, *J. Vac. Sci. Technol. A* **6**, 2175 (1988).

[10]S.G. Anderson, H.M. Meyer, III, and J.H. Weaver, *J. Vac. Sci. Technol. A* **6**, 2205 (1988).

[11]D.S. Dunn and J.L. Grant, *J. Vac. Sci. Technol. A* **7**, 253 (1989).

[12]R. Haight, R.C. White, B.D. Silverman, and P.S. Ho, *J. Vac. Sci. Technol. A* **6**, 2188 (1988).

[13]R. Haight, R.C. White, B.D. Silverman, and P.S. Ho, *Appl. Phys. Lett.* **51**, 481, (1987).

[14]P.N. Sanda, J.W. Bartha, J.E. Clobis, J.L. Jordan, C. Feger, B.D. Silverman, *J. Vac. Sci. Technol. A* **4**, 1035 (1986).

[15]F.K. LeGoues, B.D. Silverman, and P.S. Ho, *J. Vac. Sci. Technol. A* **6**, 2200 (1988).

[16]H.M. Meyer, III, S.G. Anderson, Lj. Atanasoska, and J.H. Weaver, *J. Vac. Sci. Technol. A* **6**, 2175 (1988).

[17]H. Dannenberg, *J. Appl. Polymer Sci.* **5**, 125 (1961).

[18]M. L. Williams, *J. Appl. Polymer Sci.* **13**, 29 (1969).

[19]M. L. Williams, *J. Appl. Polymer Sci.* **14**, 1121 (1970).

[20]J. D. Burton, W. B. Jones, and M. L. Williams, *Trans. Soc. Rheolog,* **15**, 39 (1970).

[21]G. P. Anderson, K. L. DeVries, and M. L. Williams, *J. Colloid Interface Sci.* **47**, 600 (1974).

[22]G. P. Anderson, K. L. DeVries, and M. L. Williams, *Int. J. Fracture* **10**, 565 (1974).

[23]S. J. Bennett, K. L. DeVries, and M. L. Williams, *Int. J. Fracture* **10**, 33 (1974).

[24]M. Takashi, K. Yamazaki, T. Natsume, and T. Takebe, *21st Japan Cong. on Mat. Res. - Non-Metallic Mat.,* 260 (1978).

[25]M. Yamazaki and M. Takashi, *21st Japan Cong. on Mat. Res. - Non-Metallic Mat.,* 255 (1978).

[26]F. Erdogan and K. Arin, *Int. J. Eng. Sci.* **10**, 115 (1972).

[27]K.M. Liechti, *Experimental Mechanics* **25**, 255 (1985).

[28]J. A. Hinkley, *J. Adhes.* **16**, 115 (1983).

[29]A. N. Gent, and L. H. Lewandowski, *J. Appl. Polymer Sci.* **33**, 1567 (1987).
[30]M.G. Allen, and S.D. Senturia, *J. Adhes.* **25**, 303 (1988).
[31]M.G. Allen, and S.D. Senturia, *J. Adhes.* **29**, 219 (1989).
[32]Y-H. Lai, and D.A. Dillard, *J. Adhes.* **31**, 177 (1990).
[33]M.J. Neopolatino, A. Chudnovsky, and A. Moet, *J. Adhes. Sci. Technol.* **2**, 311 (1988).
[34]D.A. Dillard, and Y. Bao, *J. Adhes.* **33**, 253 (1991).
[35]K.M. Liechti, and Y-M. Liang, *Int. J. Fracture* **55**, 95-114 (1992).
[36]K-S. Kim, and N. Aravas, *Int. J. Solids Structures* **24**, 417 (1988).
[37]S. Timoshenko, and S. Woinowsky-Kreiger, *Theory of Plates and Shells*, 2nd Ed. (McGraw-Hill, New York, 1987).
[38]H.M. Jensen, *Engineering Fracture Mechanics* **40**, 475 (1991).
[39]H.M. Jensen, and M.D. Thouless, The Danish Center for Applied Mathematics and Mechanics, Report #439 (1992).
[40]J.W. Hutchinson, and Z. Suo, "Mixed Mode Cracking in Layered Materials," in *Advances in Applied Mechanics*, Ed., J. W. Hutchinson, **29**, 63-199 (1992).
[41]J.F. Dezern and C.I. Croall, NASA Technical Memorandum 104178, Langley Research Center, Hampton, VA, December 1991.
[42]G.D. Davis, C.R. Anderson, and H.M. Clearfield, *J. Vac. Sci. Technol. A* **9**, 3135 (1993).
[43]K.M. Liechti, and E. Hanson, *Int. J. Fracture* **36**, 199-217 (1988).
[44]H.C. Cao and A.G. Evans, *Mechanics of Materials* **7**, 295 (1989).
[45]J-S. Wang and Z. Suo *Acta. Metall. Mater.* **38**, 1279 (1990).
[46]K.M., Liechti and Y-S. Chai, *J. Applied Mechanics*, **59**, 295 304 (1992).
[47]N.P. O'Dowd, M.G. Stout, and C.F. Shih, *Philosophical Magazine*, in press.
[48]L.P. Buchwalter and A.I. Baise, in *Polyimides: Synthesis, Characterization and Applications, Vol. 1*, K.L. Mittal, ed., (Plenum Press, New York, 1984), p. 537.
[49]L.P. Buchwalter and R. Saraf, *J. Adhes. Sci. Technol.* **7**, 925 (1993).
[50]G.D. Davis, *Surf. Interface Anal.* **9**, 421 (1986).
[51]G.D. Davis, T.S. Sun, J.S. Ahearn, and J.D. Venables, *J. Mater. Sci.* **17**, 1807 (1982).
[52]G.D. Davis, J.S. Ahearn, L.J. Matienzo, and J.D. Venables, *J. Mater. Sci.* **20**. 975 (1985).
[53]W.C. Moshier, G.D. Davis, and J.S. Ahearn, *Corros. Sci.* **27**, 785 (1987).
[54]G.D. Davis, W.C. Moshier, J.S. Aheam, H.F. Hough, and G.O. Cote, *J. Vac. Sci. Technol. A* **5**, 1152 (1987).
[55]G.D. Davis, S.P. Buchner, W.A. Beck, and N.E. Byer, *Appl. Surf. Sci.* **15**, 238 (1983).
[56]G.D. Davis, N.E. Byer, R.A. Riedel, and G. Margaritondo, *J. Appl. Phys.* **57**, 1915 (1985).
[57]G.D. Davis, W.A. Beck, M.K. Kelly, D. Kilday, Y.W. Mo, N. Tache, and G. Margaritondo, *Phys. Rev. B.* **38**, 9694 (1988).
[58]J.C. Bierlein, S.W. Gaarenstroom, R.A. Waldo, and A.C. Ottolini, *J. Vac. Sci. Technol. A* **2**, 1102 (1984).